EPSC2018

SB9 abstracts

EPSC Abstracts
Vol. 12, EPSC2018-393, 2018
European Planetary Science Congress 2018

Basaltic asteroids: a howardites - eucrites - diogenites view

J. A. Mansour(1,2), M. Popescu (3,4,2), J. de León (3,4)
(1) Faculty of Physics, Bucharest University, 405 Atomiştilor Street, 077125 Măgurele, Romania (jadmansour96@gmail.com); (2) Astronomical Institute of the Romanian Academy, 5 Cuţitul de Argint, 040557 Bucharest, Romania; (3) Instituto de Astrofísica de Canarias (IAC), C/Vía Láctea s/n, 38205 La Laguna, Tenerife, Spain; (4) Departamento de Astrofisica, Universidad de La Laguna, 38206 La Laguna, Tenerife, Spain.

Abstract

We present a compositional classification of 374 V-types selected from the MOVIS catalogue [1]. The classification was made by comparing the V-types colors with those of a sample of 65 HED meteorites from RELAB database. We found that 51 % of the V-type asteroids can be associated with Eucrites, 29 % with Howardites and 20 % with Diogenites. From the collisional family point of view, about 100 (≈27% of the sample) asteroids belongs to (4) Vesta family, 246 asteroids (≈66%) are not assigned to any family of asteroids and the rest 28 (≈ 7%) have been associated with various other families.

1. Introduction

Basaltic asteroids are fragments of primordial bodies that went through the process of differentiation. The differentiated asteroids and igneous meteorites provide important clues to the understanding of the accretion process and the early history of the Solar System. The ≈ 500 km size asteroid (4) Vesta is the representative member of these objects which are classified as V-types.

Most of the V-types are orbiting in the inner part of the Main Belt and have been dynamically linked with Vesta through the Rheasilvia basin [2]. A fraction of the ejected fragments spread around the Main Belt while some of them were sent into near-Earth orbits. The link between the HED meteorites and the V-types has been firmly proved spectroscopically [3]. It is considered that the eucrites were part of the upper layers of the crust, the digionites of the mantle layers while the howardites are a mixture of the two [4].

Recently, new V-type asteroids have been discovered in the middle and outer part of the belt. Since these asteroids cannot be dynamically associated with Vesta it led to the idea that other differentiated parent bodies must have existed.

The aim of this paper is to explore the possibility of using NIR colours provided in MOVIS catalog, to distinguish between the howarditic, eucritic and diogenitic compositions for the asteroids classified as V-types.

1.1. Methodology

We selected the V-type candidates provided in the MOVIS-C catalogue [5]. The following constraints on the color indices errors were applied so that only objects with: (Y-J)$_{err}$ $\leq$ 0.118 , (J-Ks)$_{err}$ $\leq$0.136, (H-K)$_{err}$ $\leq$ 0.146 were selected, thus resulting in 374 V-type candidates. To classify the asteroids according to HED typologies we used several machine learning methods. The results obtained by KNN(K-Nearest Neighbor, where K is the number of nearest neighbors) proved to be the most reliable for this data set.

As a training set, we used the sample of HED meteorites spectra following the selection of [6]. This contains data for 65 meteorites out of which 13 are Diogenites, 39 Eucrites and 13 Howardites. Their spectra are available in the RELAB database and they are converted to the (Y-J), (J-H), (H-Ks), and (J-Ks) colours corresponding to VISTA filter system. Fitting the training values with the labels of each type of meteorite and iterating through different K values, a label prediction could be established for the basaltic asteroids.

To validate our approach we performed the "leave one out test" for the algorithm. The result is summarized by the confusion matrix shown in Figure 1. The algorithm manages to identify with 53% cases howardites, 92% eucrites and 76 % diogenites. The low percent of howardites identification is due to the fact that compositionally these are a mixture of eucrites and diogenites.

We compared our results with those derived from observed spectra of three objects classified as V types. We found that the compositional type matches for

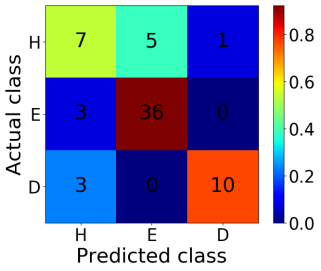

Figure 1: The confusion matrix performed for the HED data set. Probability is indicated by the color gradient

(2763) Jeans and (9064) Johndavies which are eucrites while (5952) Davemonet was classified as howardite and we predicted a diogenite like composition.

We interpreted our results in the context of proper orbital elements provided by [7].

2. Results

The classification algorithm labeled 110 asteroids as being associated to Howardites, 190 as being Eucrites and 74 Diogenites. A clear separation arises between the three groups when a (H-Ks) vs (J-H) plot is considered (Figure 2). About 100 (≈27% of the sample) asteroids belongs to (4) Vesta familly, 246 asteroids (≈66%) are not assigned to any family of asteroids and the rest of 28 (7%) objects belongs to different families including (135) Hertha, (15) Eunomia, (170) Maria, (158) Koronis, and (221) Eos.

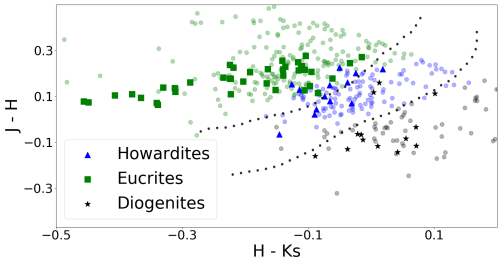

Figure 2: The colors of the asteroids(faded, circles) are correlated with the colors of the HED meteorites.

More than half of the (4) Vesta familly asteroids (53% – 53 out of 100 objects) are compatible with an eucritic composition and about 31 % have a howarditic like surface. Only 16 % of asteroids linked with (4) Vesta are compatible with diogenites, and in the orbital parameter space they are the closest to the familly parent body. Using visible and near-infrared spectra of 12 objects, [8] reported a howarditic composition in most of the vestoids.

The most common type of asteroids found are eucritic in nature regardless if they are vestoids or not while the most rare are associated with a diogenitic composition. In Figure 3 we show the distribution of this asteroid sample in the orbital parameters space. The compositional types are labeled accordingly. We note that most of the diogenites like compositions are found in the inner Main Belt, and only four objects of this type are found in the midlle part and a single diogenite like candidate was found in the outer Main Belt. This distribution does not support the existence of other basaltic families beyond 2.5 A.U.

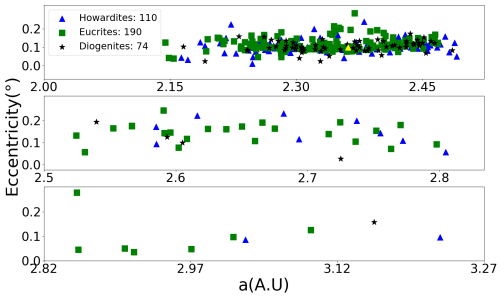

Figure 3: From top to bottom, the subplots show the distribution of the sample of asteroids in the three regions of the asteroid belt: inner, middle and outer belt. Vesta has been designated by a yellow triangle

The diogenitic like objects show slightly smaller diameters than eucritic and howarditic like objects. The vestoids classified here have diameters between ≈ 1 km and ≈ 6 km, with the largest vestoid being classified as an eucrite with a diameter of 6.9 km.

There are several hypotheses proposed to explain the basaltic asteroids in the middle and outer Main Belt. One of these considers the instability of the giant planets during migration which caused the scattering of asteroids in the Solar System. The possibility of transporting V-types due to scattering was confirmed by [9]. We note that most of the V-types in the midlle and outer part of the Main Belt have diameters less than 10 km (28 out of the total of 47 objects). They are more succeptible to be scattered objects due to Yarkovski effect but [10] and [11] deemed it unlikely.

3 Acknowledgments

This work was developed in the framework of the project PN-III-P1-1.2-PCCDI-2017-0371 financed by the Romanian National Authority for Scientific Research - UEFISCDI. The paper make use of data published by the following web-sites Minor Planet Center, and RELAB Spectral Database.

References

[1] Popescu, M.; Licandro, J.; Morate, D.; de León, J.; Nedelcu, D. A.; Rebolo, R.; McMahon, R. G.; Gonzalez-Solares, E.; Irwin, M, 2016. Near-infrared colors of minor planets recovered from VISTA-VHS survey (MOVIS) Astronomy and Astrophysics, Volume 591, id.A115, 18 pp.

[2] Thomas, P. C., Binzel, R. P., Gaffey, M. J., Storrs, A. D., Wells, E. N., Zellner, B. H. 1997. Impact excavation on asteroid 4 Vesta: Hubble Space Telescope results. Science, 277(Sept.), 1492-1495.

[3] Scott, E. R. D.; Keil, K.; Goldstein, J. I.; Asphaug, E.; Bottke, W. F.; Moskovitz, N. A, 2015. Early Impact History and Dynamical Origin of Differentiated Meteorites and Asteroids. Asteroids IV, Patrick Michel, Francesca E. DeMeo, and William F. Bottke (eds.), University of Arizona Press, Tucson, 895 pp. ISBN: 978-0-816-53213-1, 2015., p.573-595

[4] Takeda, Hiroshi, 1997 Mineralogical records of early planetary processes on the HED parent body with reference to Vesta Meteoritics and Planetary Science, vol. 32, no. 6, pages 841-853

[5] M. Popescu; J. Licandro; J. M. Carvano; R. Stoicescu; J. de León; D. Morate; I.L. Boaca; C. P. Cristescu Taxonomic classification of asteroids based on MOVIS near-infrared colors Astronomy and Astrophysics, 2018, Paper submitted

[6] Duffard, R.; Lazzaro, D.; de León, J, 2005. Revisiting spectral parameters of silicate-bearing meteorites Meteoritics and Planetary Science, Vol. 40, p.445

[7] Nesvorný, D.; Brož, M.; Carruba, V, 2015. Identification and Dynamical Properties of Asteroid Families Asteroids IV, Patrick Michel, Francesca E. DeMeo, and William F. Bottke (eds.), University of Arizona Press, Tucson, 895 pp. ISBN: 978-0-816-53213-1, 2015., p.297-321

[8] De Sanctis, Maria Cristina; Ammannito, Eleonora; Migliorini, Alessandra; Lazzaro, Daniela; Capria, Maria Teresa; McFadden, Lucy, 2011. Mineralogical characterization of some V-type asteroids, in support of the NASA Dawn mission Monthly Notices of the Royal Astronomical Society, Volume 412, Issue 4, pp. 2318-2332.

[9] P. I. O. Brasil, F. Roig, D. Nesvorny and V. Carruba, 2017 Scattering V-type asteroids during the giant planets instability: A step for Jupiter, a leap for basalt. AA(Observatório Nacional, 20921-400 Rio de Janeiro, RJ, Brazil), AB(Observatório Nacional, 20921-400 Rio de Janeiro, RJ, Brazil), AC(Southwest Research Institute, Boulder, CO 80302, USA), AD(Faculdade de Engenharia, Universidade Estadual Paulista, 12516-410 Guaratinguetá, SP, Brazil)

[10] Roig, F.; Nesvorný, D.; Gil-Hutton, R.; Lazzaro, D, 2008. V-type asteroids in the middle main belt Icarus, Volume 194, Issue 1, p. 125-136.

[11] Folonier, H. A.; Roig, F.; Beaugé, C, 2014. Capture probability in the 3:1 mean motion resonance with Jupiter: an application to the Vesta family Celestial Mechanics and Dynamical Astronomy, Volume 119, Issue 1, pp.1-25

EPSC Abstracts
Vol. 12, EPSC2018-449, 2018
European Planetary Science Congress 2018

The Geology of Ceres and Vesta

K. Krohn (1), R. Jaumann (1,2) D. L. Buczkowski (3), D. A. Williams (4), M.C. De Sanctis (5), C. M. Pieters (6), K. A. Otto (1), O. Ruesch (7), K. Stephan (1), F. Tosi (5), R. J. Wagner (1), F. Zambon (5), C. A. Raymond (8), C. T. Russell (9), and the Dawn Science Team

(1) Institute of Planetary Research, German Aerospace Center (DLR), Berlin, Germany (Katrin.Krohn@dlr.de); (2) Freie Universität Berlin, Inst. of Geosciences, Planetology and Remote Sensing; (3) Johns Hopkins University Applied Physics Laboratory Laurel, USA; (4) Arizona State University, Tempe, USA; (5) INAF-IAPS, National Institute for Astrophysics, Rome, Italy, (6) Brown University, Providence, RI, USA; (7) ESTEC, European Space Agency, Noordwijk, The Netherlands; (8) NASA JPL, California Institute of Technology, Pasadena, California, USA, (9) UCLA, Los Angeles, California, USA. (Katrin.krohn@dlr.de)

1. Introduction

In 2007 the Dawn spacecraft was launched into space in order to study the two most massive objects of the asteroid belt: Vesta and Ceres. The goal of the mission was to understand the conditions and processes that formed the early solar system on the basis of the geology, elemental and mineralogical composition, topography, shape, and internal structure of Vesta and Ceres. In July 2011 Dawn entered orbit around Vesta and started a complete survey of the south polar and equatorial regions with Survey and High Altitude Mapping (HAMO) data (Russell et al., 2012). The high resolution Low Altitude Mapping (LAMO) data nearly covers the surface of Vesta from 90°S up to 55°N for about 90%. After studying Vesta for 14 months with its Framing Camera (FC) [2], Visible- and Infrared Spectrometer (VIR) [3] and Gamma-Ray and Neutron Detector (GRaND) [4], NASA's Dawn spacecraft departed Vesta in September 2012 and entered orbit around Ceres on March 6, 2015, where it still remains. Dawn recently finished its global mapping at Ceres and continues there with an extended mission. The main geologic results of the two bodies are described below.

2. Geologic features on Vesta

Vesta's surface reveals a multifaceted morphology with impact basins, various forms of impact craters, a variety of ejecta blankets, large troughs extending around the equatorial region, enigmatic dark material, mass wasting features and surface alteration processes [5-7]. The south polar region is dominated by two large impact basins, Veneneia underlying the larger Rheasilvia basin [5,6]. They are strongly correlated with Vesta's global tectonic patterns, the two distinct sets of large trough-and groove terrrains named Saturnalia and Divalia Fossae, respectively, and may have formed them [5,7]. Overall, Vesta shows a complex topography with extreme height differences resulting in steep slopes, locally exceeding 40° [8]. Comparable to the Moon, impact craters on Vesta range from fresh to highly degraded, indicating an intensive cratering history [5,6]. The steep sloped topography of Vesta results in craters with an unusual asymmetrical shape, where a sharp crater rim exists on the uphill side, and a subdued rim on the downhill side [8]. The asymmetrical shape was formed because of the preferential accumulation of ejecta material on the downhill crater rim relative to the uphill rim [8]. Other remarkable features associated with craters or steep slopes on Vests are pitted terrains and gullies. Pitted terrains are found in young craters and are interpreted to be the result of outgassing of volatile-rich material [9]. Linear gullies are interpreted to be formed by flow of dry granular material and curvilinear gullies are possibly formed by transient flow of water [10]. HED meteorites (Howardite-Eucrite-Diogenite) are believed to originate from Vesta [14, and ref's therein].

Most of the Vestan surface is composed of Howardite material with localized enrichments of Eucrite and Diogenite [11,12]. The surface of Vesta consists of thick (100 meters to a few kilometers), multilayered sheets of regolith with different albedos, formed by the accumulation of ejecta from numerous impacts that have resurfaced Vesta over time [5,13]. Deposits of dark material are intermixed into the regolith, and partially were excavated by impacts. They are exposed as dark halos around craters, or blocks and layers out-cropping in crater walls and rims [5,13], indicating material was excavated from the subsurface. The distribution of dark material

seems to be correlated with the rim and ejecta of Veneneia, which match with the hypothesis that the dark material is exogenic, from carbon-rich low velocity impactors. Nevertheless, an endogenic origin, from freshly exposed mafic material or impact melt, exposed or produced by impacts is also possible. The correlation between dark material and an OH hydration band, indicate the presence of carbonaceous chondrites [5,13-16]. However, the bright ejecta material found on Vesta´s surface is thought to represent fresh, unweathered surface material [15,17].

3. Geologic features on Ceres

Prior to the Dawn Mission, Ceres, the dwarf planet was anticipated to be dark, wet and at least partially differentiated [18]. The surface of Ceres reveals a wide range of different features which are interpreted to be formed by water ice and/or volatile-rich material, e.g., domes, pits, plains and lobate flows [19-23]. The 4-km- high Ahuna Mons is the most prominent dome on Ceres and thought to be formed by the extrusion of cryolavas [21]. Cryolava is also found within Occator crater. The bright material of the faculae within Occator is thought to consist of liquid brine, rich in carbonates and ammoniated salts. Liquid brines are thought to reach the surface at high velocity, as in a salt-water fountain [24]. Young craters shows a bluish signature in the enhanced FC HAMO color mosaics (956/555/440 nm) [20,25]. The blue material implies a possible relationship to an impact-triggered alteration and/or space weathering processes, that could be linked with blankets of ultrafine grains and partly amorphous phyllosilicates [24]. Ceres´ surface is disrupted by numerous linear features, which are thought to be impact-derived secondary crater chains or fractures and faults [19,26].

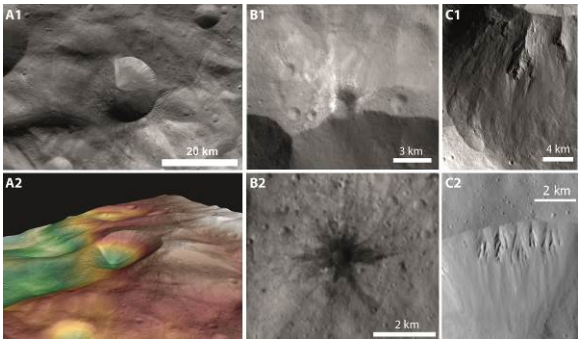

Figure 1: Examples of features on Vesta: A1+2: Asymmetric crater Antonia. B1: Bright material. B2: dark material. C1+2: Spur-and gully morphology.

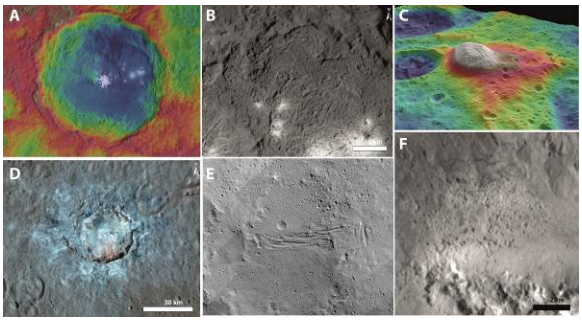

Figure 2: Examples of features on Ceres: A: Occator crater and its faculae. B: Flow features within Occator. C: Ahuna Mons. D: Blue material at Haulani. E: Cracks within Yalode crater. F: Pits within Haulani.

Acknowledgements

We thank the Dawn team for the development, cruise, orbital insertion, and operations of the Dawn spacecraft at Ceres. K. Krohn is supported by the Helmholtz Association (HGF) through the research Helmholtz Postdoc Program.

References

[1] Russell, C.T. et al., 2012, Science 336; [2] Sierks, H. et al., 2011, SSR 163, 263-327. [3] De Sanctis, M.C. et al., 2011, SSR 163, 329–369. [4] Prettyman et al., 2011, SSR 163, 371–459. [5] Jaumann, R., et al., 2012, Science 336, 687-690. [6] Schenk P., et al., 2012, Science 336, 964-967. [7] Buczkowski, D., et al., 2012, GRL, 39, L18205. [8] Krohn et al., 2014, PSS 103, 36-56. [9] Denevi B. W. et al. (2012), Science, 338. [10] Scully J.E.C. et al. (2015), EPSL, 411. [11] Prettyman T. H. et al. (2012), Science, 338. [12] De Sanctis M. C.et al.(2012), ApJ, 758. [13] Jaumann. R. et al., 2014, Icarus 240, 3-19. [14] McCord,T. B. et al., 2013, Nature 491, 83-86. [15] Stephan, K. et al., 2014, JGR 119, 771-797. [16] De Sanctis et al., 2012, Ap.J.L., 758: L36. [17] Zambon, F. et al., 2014, Icarus 240, 73-85. [18] Russell C. T. et al., 2016, Science 353, 1008-1010. [19] Buczkowski, D. L. et al., 2016, Science 353. [20] Krohn, K. et al., 2016, GRL 43. [21] Ruesch, O. et al., 2016, Science 353. [22] Schmidt, B. et al., 2017, Nat. Geo. Sci. 10. [23] Sizemore, H. et al., 2017, GRL, 44. [24] Ruesch et al., 2018, Icarus. [25] Stephan, K. et al., 2017, GRL 44. [26] Scully, J. E. C., 2017, GRL 44.

EPSC Abstracts
Vol. 12, EPSC2018-484, 2018
European Planetary Science Congress 2018

Search for water outgassing of (1) Ceres near its perihelion

P. Rousselot (1), C. Opitom (2), E. Jehin (3), D. Hutsemékers (3), J. Manfroid (3), M.N. Villarreal (4), J.-Y Li (5), J. Castillo-Rogez (6), C.T. Russell (4), P. Vernazza (7), M. Marsset (8), L. Roth (9), C. Dumas (10), B. Yang (2,11), O. Mousis (7)
(1) Institut UTINAM UMR 6213, CNRS, Univ. Bourgogne Franche-Comté, OSU THETA, BP 1615, 25010 Besançon Cedex, France (phil@obs-besancon.fr), (2) European Southern Observatory, Alonso de Còrdova 3107, Vitacura Casilla 19001, Santiago, Chile, (3) Space sciences, Technologies & Astrophysics Research (STAR) Institute, University of Liège, Liège, Belgium, (4) Earth, Planetary and Space Sciences, University of California, Los Angeles, 405 Hilgard Avenue, Los Angeles, CA 90095-1567, USA, (5) Planetary Science Institute, 1700 E Fort Lowell Road, Tucson, AZ 85719, USA, (6) Jet Propulsion Laboratory, California Institute of Technology, Pasadena, CA 91109, USA, (7) Aix Marseille Univ, CNRS, LAM, Laboratoire d'Astrophysique de Marseille, Marseille, France, (8) Astrophysics Research Centre, Queen's University Belfast, Belfast, County Antrim, BT7 1NN, UK, (9) School of Electrical Engineering, KTH Royal Institute of Technology, Stockholm, Sweden, (10) Thirty-Meter-Telescope, 100 West Walnut St, Suite 300, Pasadena, CA 91124, USA, (11) Yunnan Observatories, Chinese Academy of Sciences, Kunming 650011, PR China

Abstract

(1) Ceres is the largest body in the main asteroid belt and one of the most intriguing object since the discovery of water outgassing in the infrared by the Herschel space observatory in 2014. Ceres is the current target of NASA's Dawn spacecraft. Recently, the possible influence of the local flux of solar energetic particles (SEP) on the production of a cerean exosphere and water vapor has been suggested. On the other hand the Herschel, IUE and ground-based observations seem to show a correlation between water vapor emission and Ceres heliocentric distance. We used the opportunity of both the perihelion passage of (1) Ceres in 2018 and the presence of Dawn in its vicinity (for measuring the SEP flux in real time) to check the influence of heliocentric distance on water outgassing. We searched for OH emission lines from the limb of Ceres in the near-UV. Despite a sensitivity level similar to the Herschel observations we did not detect any water outgassing.

1. Introduction

Among the numerous asteroids in the main belt, Ceres is one of the most interesting object. This is due to the fact that it is the largest one (average diameter of 940 km from the Dawn results, it is the only dwarf planet in the main belt) and it presents unusual physical characteristics. The most intriguing of them is the possible water outgassing. This outgassing was first marginally detected with OH emission lines in the near-UV by [1] but not confirmed by [8] with the same lines. Finally water was directly detected through absorption of the continuum from Ceres in an H_2O infrared line by the Herschel satellite [5]. HST observations also searched for the atomic oxygen emission lines but failed, nevertheless, to detect water outgassing [7]. Because the sensitivity of the observations of these different works was similar, it is clear that water outgassing is a transient phenomenon on the surface of Ceres. The possible influence of the local flux of SEP on the apparition of a cerean exosphere and water vapor has also been suggested [10].

Water outgassing is consistent with the expected internal structure of Ceres. This body is differentiated into a silicate core and an icy mantle [4], while hydrated minerals have been found ubiquitous on its surface [6][3] and water ice has also been detected [2]. Its low density, 2.162 ± 0.003 g.cm^{-3} [9], suggests a high content of ice up to 30%, if its porosity is low.

The physical mechanism responsible for water outgassing being unclear, it was the objective of this work to get new observational constraints during the perihelion passage of Ceres in 2018.

2. Observations

Ceres was observed on February 16, 2018 at the European Southern Observatory (ESO) using the 8.2-m UT2/Kueyen telescope of the Very Large Telescope (VLT) with the Ultraviolet and Visual Echelle Spectrograph (UVES) instrument. This instrument is a cross-dispersed echelle spectrograph designed to operate with high efficiency from the atmospheric cut-off at 300 nm to the long wavelength limit of the CCD detectors (about 1100 nm). To this aim, the light beam

from the telescope is split in two arms (UV to Blue, and Visual to Red) within the instrument. Ceres was observed with the Blue arm centered at 346 nm, with a resolving power $\lambda/\Delta\lambda \simeq 15,000$.

The slit was oriented perpendicular to Ceres spin axis, above the northern hemisphere, Ceres being positioned outside the slit with an offset of 6 arcsec with respect to the slit center. The slit width was 3 arcsec. Two spectra were obtained with a similar exposure time of 4815 s. At that time Ceres heliocentric distance was 2.566 au and geocentric distance 1.63 au (Ceres heliocentric distance varying from 2.556 to 2.978 au).

Simultaneously to these VLT observations, the GRaND experiment, onboard the Dawn spacecraft orbiting around Ceres, measured the energetic proton flux near Ceres. Despite a SEP event detected around Earth on February 12 by the NASA Advanced Composition Explorer satellite, GRaND did not measure a significant increase of energetic proton flux near Ceres at the time of our observations. So, if water outgassing on Ceres is due to a SEP event, such an event was not occurring during our observations.

3. Data analysis

The two spectra obtained have been processed in a standard manner (i.e. wavelength and flux calibrated). The two 2D spectra were converted in 1D spectra by co-adding the 38 different lines corresponding to the slit length (38×0.25=9.5 arcsec). We computed a synthetic OH spectrum for the heliocentric distance and velocity of Ceres at the time of observations and searched for these lines in the observational spectra.

No OH lines could be detected directly. We also co-added all the parts of the observational spectra where OH lines were expected, in order to improve the signal-to-noise ratio as much as possible. Once again no OH could be detected.

A first estimate of the upper limit for the OH production rate lead to $Q_{max} \simeq 10^{26}$ molecules.s^{-1}, i.e. the same order of magnitude that the production rate measured by Herschel.

4. Conclusions

From previous observations, water outgassing on Ceres seems to be a transient phenomenon that could be due either to solar heating - as for comets - or to the influence of SEP events. Because of the lack of positive detection during our observations, performed both near perihelion and with no energetic particles hitting the surface of Ceres, this work adds support to the influence of SEP activity for triggering water outgassing. Nevertheless, complementary observations, ideally conducted during such an event, are necessary to reach a definitive conclusion.

Acknowledgements

Based on observations collected at the European Southern Observatory, Paranal, Chile (observing proposal 2100.C-5038).

References

[1] A'Hearn, M. and Feldman, P.D.: Water vaporization on Ceres, Icarus, 98, pp. 54-60, 1992

[2] Combe, J.-P., McCord, T.B., Tosi, F., et al.: Detection of local H_2O exposed at the surface of Ceres, Science, 353, id.aaf3010, 2016

[3] de Sanctis, M.C., Ammannito, E., Raponi, A., et al.: Ammoniated phyllosilicates with a likely outer solar system origin on (1) Ceres, Nature, 528, pp 241-244, 2015

[4] Ermakov, A. I., Fu, R. R., Castillo-Rogez, J. C., et al.: Constraints on Ceres' Internal Structure and Evolution From Its Shape and Gravity Measured by the Dawn Spacecraft, JGR 122, pp. 2267-2293, 2017

[5] Küppers, M., O'Rourke, L., Bockel 'e-Morvan, D., et al.: Localized sources of water vapour on the dwarf planet (1) Ceres, Nature, 505, pp. 525-527, 2014

[6] McCord, T.B., Castillo-Rogez, and J., Rivkin, A.: Ceres: its origin, evolution and structure and Dawn's potential contribution, Space Science Reviews, 163, pp. 63-76, 2011

[7] Roth, L., Ivchenko, N., Retherford, K.D., et al.: Constraints on an exosphere at Ceres from Hubble Space Telescope observations, GRL, 43, pp 2465-2472, 2016

[8] Rousselot, P., Jehin, E., Manfroid, J., et al.: A search for water vaporization on Ceres, AJ, 142, id. 125 (6pp), 2011

[9] Russell C.T., Raymond, C.A., Ammannito, E., et al.: Dawn arrives at Ceres: exploration of a small, volatile-rich world, Science, 353, pp. 1008-1010, 2016

[10] Villarreal, M.N., Russell, C.T., Luhmann, J.G., et al.: The dependence of the cerean exosphere on solar energetic particles events, ApJL, 838, L8 (5pp), 2017

EPSC Abstracts
Vol. 12, EPSC2018-555, 2018
European Planetary Science Congress 2018

Temperature and emissivity of specific regions of interest on Ceres

F. Tosi (1), M. T. Capria (1), E. Rognini (1), M. C. De Sanctis (1), M. Formisano (1), G. Thangjam (2), F. Zambon (1), E. Ammannito (3,1), F. G. Carrozzo (1), M. Ciarniello (1), J.-Ph. Combe (4), K. Krohn (5), A. Longobardo (1), A. Nathues (2), E. Palomba (1), A. Raponi (1), K. Stephan (5), C. A. Raymond (6), and C. T. Russell (7).

(1) INAF-IAPS Istituto di Astrofisica e Planetologia Spaziali, Via del Fosso del Cavaliere 100, I-00133 Rome, Italy, federico.tosi@iaps.inaf.it. (2) Max Planck Institute for Solar System Research, Göttingen, Germany. (3) Agenzia Spaziale Italiana, Rome, Italy. (4) The Bear Fight Institute, Winthrop, WA, USA. (5) Institute of Planetary Research, German Aerospace Center (DLR), Berlin, Germany. (6) NASA/Jet Propulsion Laboratory and California Institute of Technology, Pasadena, CA, USA. (7) University of California at Los Angeles, Los Angeles, CA, USA.

Abstract

We describe the thermal behavior of some notable features, investigated by the Dawn spacecraft on the dwarf planet Ceres, using thermal infrared data acquired by the Visible and InfraRed mapping spectrometer (VIR), and comparing them with the local geology and mineralogy of those areas. Based on experience gained at Vesta, thermal information at unprecedented spatial resolution is useful in constraining thermophysical properties, which ultimately allow a comprehensive interpretation of the observed features.

In this paper we summarize the most salient results concerning the thermal analysis of Ceres, and we will present preliminary results of the thermal analysis obtained for the latest VIR data obtained during Dawn's second extended mission (XM2).

1. Introduction

The NASA Dawn spacecraft entered orbit around the dwarf planet Ceres in March 2015, where it is currently approaching its end-of-mission. In the mission phases that have been planned, the VIR imaging spectrometer aboard Dawn acquired a large amount of hyperspectral data of the surface, to map the surface composition and to retrieve surface temperatures on the dayside of the target.

The infrared range longward of ~3.5 μm is crucial to reveal the thermal emission of Ceres on its dayside, which can be used to map surface temperature across different orbits and local solar times (LST), and therefore constrain thermal properties at different spatial scales.

To derive surface temperature, we rely on a Bayeasian approach to nonlinear inversion that was applied to different datasets: 1) Dawn/VIR data acquired during the orbital phase at asteroid Vesta in 2011-2012 [1], 2) Rosetta/VIRTIS data obtained during the close flyby of asteroid 21 Lutetia in 2010 [2], and 3) Rosetta/VIRTIS data acquired at comet 67P/Churyumov-Gerasimenko in the two-year period 2014-2015 [3]. Compared to other methods, this approach allows simultaneous retrieval of surface temperature and emissivity in the 4.5-5.1 μm range.

2. Results

On Ceres, the feature displaying the largest thermal contrast, both on a regional and local scale, is the 34-km crater Haulani, located in the equatorial region and close to the prime meridian. Its central mountainous ridge, its floor, rim and its nearest ejecta appear cooler than surrounding terrains observed under similar illumination conditions and LST [4]. While Haulani is one of the youngest surface features of Ceres (< 6 Myr), its thermal contrast is not as distinct as in other young craters like Oxo, Juling and Kupalo, difficult to be explained with space weathering. Rather, the characteristics of the impact event that formed crater Haulani, also triggering hydrothermal activity in the shallow subsurface, could have exposed material with higher density or different thermal conductivity compared to other similar young impact features. An accurate thermophysical modeling of Haulani will allow one to identify the main cause of the thermal signature that is unique to crater Haulani [5].

Bright material units were discovered on Ceres by the Dawn spacecraft during approach in early 2015.

The brightest cluster of spots is found in the 92-km complex Occator crater. VIR data acquired in the near infrared revealed that Cerealia Facula (the brightest spot) is made up of an outcrop of anhydrous sodium carbonate, which is the solid residue of crystallization of brines erupted from below. Despite their compositional uniqueness on Ceres, Occator's faculae do not show substantial thermal contrast at spatial resolutions of kilometers down to a few hundreds of meters, suggesting that albedo does not strongly constrain surface temperature on Ceres.

Dawn/VIR spectra allowed a safe identification of water ice-rich materials on the surface of Ceres. Starting from the 10-km crater Oxo [6], a total of about ten ice-rich units were discovered in as many craters located poleward of 30°. These units are favored by peculiar local topography, which allows ice to be shielded from direct sunlight for most of the Cerean day, or are the result of recent impacts or recent landslide activities [7]. In this respect, crater Juling is particularly interesting since the extension of its ice-rich unit has been discovered to change with time, suggesting a potential connection with the sporadic variations of water and hydroxyl observed from space [8]. Because pure surficial H2O ice would sublime under current thermal conditions on Ceres, where daytime surface temperatures span the range 180-245 K, direct thermal mapping enabled by VIR infrared data can put constraints on the ice loss rate of ice-rich materials, helping us to constrain their formation and retention mechanism.

With an average height of about 4 km, Ahuna Mons is the highest mountain discovered on Ceres. A thermal analysis of Ahuna Mons carried out with VIR highlights that the northern flank and the summit of Ahuna could be inherently cooler than the surrounding regions observed at the same local time [9]. Ahuna is hypothesized to be cryovolcanic in origin, and its sodium carbonate-rich mineralogy and morphologically fresh features support a relatively young age of this particular area though the formation age of the Mons is ~200 Ma [10]. This evidence of younger age and the association with thermal anomaly could be related to a different compactness of the surface regolith.

In addition to presenting a summary of the main discoveries made by Dawn/VIR in the thermal mapping of Ceres, here we will also present preliminary results related to the spectral emissivity retrieved for the main structures previously discussed. Because Dawn's second extended mission (XM2) is carried out on an elliptical orbit that provides the opportunity to overfly features of interest such as craters Juling, Occator and Haulani with unprecedented pixel resolution, we will attempt a thermal analysis of those data.

Acknowledgements

This work is supported by the Italian Space Agency (ASI, ASI-INAF n. I/004/12/1) and NASA. Enabling contributions from the Dawn Instrument, Operations, and Science Teams are gratefully acknowledged. The computational resources used in this research have been supplied by INAF-IAPS through the DataWell and Cyborg distributed processing facilities.

References

[1] Tosi, F., et al. (2014). Thermal measurements of dark and bright surface features on Vesta as derived from Dawn/VIR. Icarus 240 (2014) 36–57. DOI: 10.1111/maps.13078.

[2] Keihm, S., et al. (2012). Interpretation of combined infrared, submillimeter, and millimeter thermal flux data obtained during the Rosetta fly-by of Asteroid (21) Lutetia. Icarus 221 (2012) 395–404. DOI: 10.1016/j.icarus.2012.08.002.

[3] Tosi, F., et al. (2018). Surface temperature and physical properties of the nucleus of comet 67P/CG. Submitted to Nat. Astron. Under review.

[4] Tosi, F., et al. (2018). Mineralogy and temperature of crater Haulani on Ceres. Meteorit. Planet. Sci., in press. DOI: 10.1111/maps.13078.

[5] Rognini, E., et al. (2018). Ceres' thermal inertia from Dawn data. In preparation.

[6] Combe, J.-Ph., et al. (2016). Detection of local H2O exposed at the surface of Ceres. Science 353 (6303), aaf3010 (2016). DOI: 10.1126/science.aaf3010.

[7] Combe, J.-Ph., et al. (2017). Exposed H2O-rich areas detected on Ceres with the Dawn visible and infrared mapping spectrometer. Icarus, in press. DOI: 10.1016/j.icarus.2017.12.008.

[8] Raponi, A., et al. (2018). Variations in the amount of water ice on Ceres' surface suggest a seasonal water cycle. Sci. Adv. 2018;4:eaao3757. DOI: 10.1126/sciadv.aao3757.

[9] Zambon, F., et al. (2017). Spectral analysis of Ahuna Mons from Dawn mission's visible-infrared spectrometer. Geophys. Res. Lett. 44 (1), 97–104. DOI: 10.1002/2016GL071303.

[10] Ruesch, O., et al. (2016). Cryovolcanism on Ceres. Science 353 (6303), id.aaf4286. DOI: 10.1126/science.aaf4286.

EPSC Abstracts
Vol. 12, EPSC2018-606-1, 2018
European Planetary Science Congress 2018

Laccolithic "Pingo" & Hydrothermal Origins for the Central Features of Occator Crater, Ceres

P. Schenk (1), H. Sizemore (2), B. Schmidt (3), T. Bowling (4), J. Castillo-Rogez (5), C. Raymond (5), and Dawn Science Team
(1) Lunar and Planetary Institute, Houston, TX, USA, (schenk@lpi.usra.edu) (2) Planetary Science Institute, Tucson, AZ, (3) Georgia Tech. University Atlanta, GA, (4) Southwest Research Institute, Boulder, CO, (5) Jet Propulsion Lab, Pasadena, CA.

Abstract

Dawn mapping of Occator crater Ceres indicates that the carbonate-rich deposits at its center are related to formation of the central pit and central dome within it. Spatial associations indicate that the deposit may have been associated with discrete venting sources, at least at several sites, and that the dome formed after the deposit was (mostly) in place. The dome was probably formed by laccolithic-style inflation from below, perhaps due to the forced migration of water-rich fluids toward the center (and the sources of the deposit) followed by freezing.

1. Introduction

The carbonate deposits at Occator crater, Ceres, are spatially and temporally associated with the central structure of that 92-km diameter fresh complex impact crater. The deposits lie within a 10-km wide central pit featuring a fractured central dome. Here, in advance of extended mission mapping, we examine the morphologic evidence in support of an origin related to hydrothermally driven deposition of carbonates and subsequent inflation of the central dome from beneath.

2. Origins of Cerealia Facula

Hydrothermal venting of mineral-rich fluids at the center of Occator (and presumably other large craters in the past) on Ceres has been proposed for the bright materials on Occator (e.g., 1, 2, 3). These fluids would be driven by the decay of residual heating in the center of the crater (4).

The process(es) of emplacement of the carbonate-rich deposits at Occator are fundamental and yet very poorly understood in the current 35-m resolution images. No obvious central vent has been identified. Bright material extends up the inward-facing walls of the central pit, forming tendrils or lobate extensions. In numerous locations in the western quadrant (though not all), bright material clearly extends downslope from several elongate ridge-like dark features (Fig. 1). In another location part way up the sides of a steep-sided plateau (Fig. 1), bright material also appears to emanate from a row of dark spots. Both examples suggest outflow from one or more specific horizons. These are the best candidates for the formation of carbonate deposits from the outflow of fluids from discrete sources.

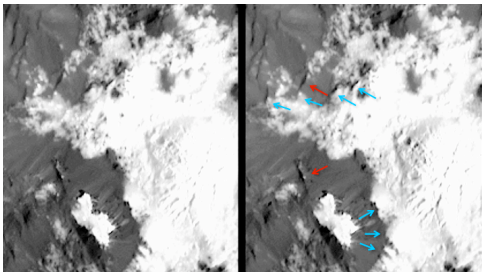

Figure 1: Enlargement and contrast enhancement, highlighting narrow ridge-like structures (blue arrows) and dark spots along outer edge of the bright materials along western margins of Cerealia Facula; candidate vent sources for hydrothermal venting. Resolution ~35 m/pixel.

3. Origins of the Central Dome

The timing of the formation of the dome in Occator is key to understanding the sequence of events. The fracture network on its surface (Fig. 2) occurs only on the dome itself and does not (with rare exception) extend up onto the pit walls. Similarly, the southern flank of the dome is also stratigraphically contiguous with bright deposits on the pit walls. The northern contact between dome and pit is more complex but does not appear to require different materials. These suggest that doming occurred after Cerealia Facula was (mostly) emplaced, that doming was limited to a

small area only 3-4 km wide, and that doming was not the result of extrusion of new material.

The stratigraphy of the central dome suggests that a laccolithic model is most likely for the dome. Laccoliths can form from intrusion of new material in one location. The material can be in the solid or liquid state. The most common examples include magma bodies, salt domes and pingos. Fracturing of overburden rocks can often produce fracture patterns (5) very similar to those observed at Occator.

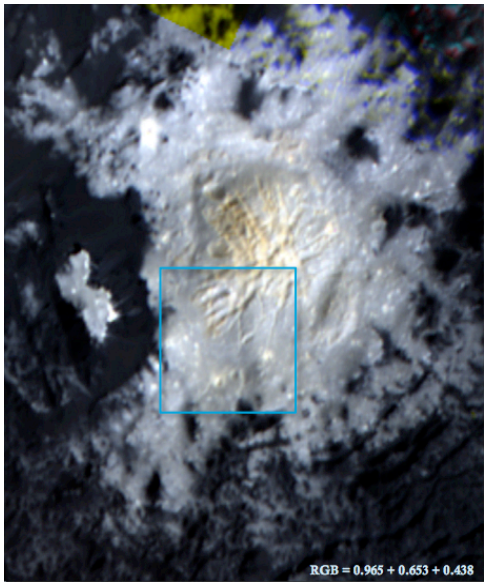

Figure 2: Fractured central dome, Occator crater. Box highlights transition from dome to central pit wall, with no apparent break in stratigraphy.

Without direct observations of the intruding material we are forced to speculate regarding candidate dome-forming processes and materials. Calculations indicate that temperatures above melting point of water are probable beneath the crater (4). Mineral-rich fluids can then be formed by mixing or leaching of more rocky materials by water, followed by migration towards the warmest surfaces (i.e., the center) (e.g., 9). Salt domes are one candidate but they tend to be rather dry.

Pingos are domical polar features formed in permafrost zones experiencing diurnal or seasonal freeze-thaw cycles (6) (7). These cycles allow or even force the migration of liquid water to local topographic or structural deviances, where it accumulates as part of the freeze-thaw cycle. On Ceres, this could be driven as well by the radially inward freezing cycle beneath crater floor, centered on the region of the central pit where the bedrock is most fractured (8) and topography is lowest.

4. Summary and Conclusions

Analysis of Dawn imaging points to hydrothermal outgassing of mineral-rich fluids from the beneath the central pit of Occator crater. The dome on the floor of the pit suggests a complex process of either freezing of water-rich fluids beneath the dome or intrusion of water-rich materials that subsequently froze. The volume of the dome is on the order of 2.75 km^3, indicating that the amount of mobilized fluids was limited.

References

[1] de Sanctis, M., et al., A Possible Brine Reservoir Beneath Occator Crater: Thermal and Compositional Evolution and Formation of the Cerealia Dome and Vinalia Faculae, Nature, 528, 241-244, 2016.

[2] Quick, L. et al., Icarus, in press, 2018.

[3] Schenk, P. et al., Icarus in press, 2018.

[4] Bowling, T., et al., Icarus, in press, 2018.

[5] Yin, H, and R. Groshong, Balancing and restoration of piercement structures: geologic insights from 3D kinematic models, J. Struct. Geology, 28, 99-114, 2006.

[6] Holmes, W., D. Hopkins, and H. Foster, Pingos in Central Alaska, Geol Survey. Bull. 1241-H, 1968.

[7] Mackay, J. R., Pingo growth and collapse, Tuktoyaktuk Pensinsula, Geogr. Physique et Quatr., 52, 10.7202/004847ar.

[8] Kenkmann, T., G. S. Collins, and K. Wünnemann, The modification stage of crater formation, in Impact Cratering: Processes and Products, pp. 60–75, 2012.

[9] Barnhart, C., F. Nimmo, and B. Travis, Martian post-impact hydrothermal systems incorporating freezing, Icarus, 208, 101-117, 2010.

EPSC Abstracts
Vol. 12, EPSC2018-612, 2018
European Planetary Science Congress 2018

Dawn's Second Extended Mission at Ceres: A New Perspective

Julie Castillo-Rogez (1), Carol Raymond (1), Christopher Russell (2), Thomas Prettyman (3), Maria Cristina De Sanctis (4), Andreas Nathues (5), Ryan Park (1), Carol Polanskey (1), Steve Joy (2), Marc Rayman (1), and the Dawn Team
(1) Jet Propulsion Laboratory, California Institute of Technology, Pasadena, CA, USA, (2) University of California Los Angeles, IGPP/EPSS, Los Angeles, CA, USA, (3) Planetary Science Institute, Tucson, AZ, USA. (4) IAPS/INAF, Rome, Italy, (5) MPS, Göttingen, Germany, (Julie.C.Castillo@jpl.nasaa.gov).

Abstract

Dawn completed its primary mission, achieving all of its Level-1 requirements, in June of 2016 after spending 7 months in a low altitude mapping orbit (LAMO) at ~385 km distance to the surface. NASA approved a one-year extension of mission operations (XM1) at Ceres, between June 2016 and October 2017, to refine the primary mission data sets and obtain repeat observations to look for surface changes. The objectives of XM1 were achieved with sufficient hydrazine remaining on the spacecraft to support continued operations [1]. In October 2017, NASA approved a second extended mission for Dawn at Ceres (XM2), spanning perihelion passage (April 2018), to obtain new high-priority science data until the spacecraft runs out of hydrazine. At the time this abstract is being written, Dawn is on its way to its final orbit.

1. Dawn's Second Extended Mission

The primary science objective of XM2 is for Dawn to obtain elemental concentrations with high sensitivity and at the scale of geological units. Proximity to the target is key to improving the strength of the gamma ray and neutron signals, as well as improving the ability to spatially resolve the elemental variations. Considerable work and ingenuity by the Dawn Flight team has produced an eccentric orbit with periapsis lower than 50 km, enabling GRaND to directly measure the elemental composition of surface units with spatial resolution at least 7x better than in LAMO orbit. The measurements will occur during a particularly quiet period of solar activity so that the intensity of galactic cosmic rays, used to interrogate the surface, is maximum. This is indeed a perfect timing for this type of investigation.

Limited longitudinal coverage will be obtained in a resonant orbit that focuses on Occator crater and its ejecta, while also characterizing the ancient heavily cratered terrains in the north, and the more recent, large Urvara and Yalode basins in the south. Combining these very low altitude data with the extended background time series obtained during XM1 will improve the entire GRaND data set and yield a deeper understanding of surface geochemistry, including the concentration and distribution of subsurface ice, as well as the elemental concentration of the ice-free regolith. Comparison between very old terrains and material recently excavated from Ceres' crust will bring new insights into the origin of Ceres' surface, an open question at this time. Furthermore, imaging with the framing camera (FC) and infrared spectra with the visible and infrared mapping spectrometer (VIR) will bring additional perspectives on Ceres' geological evolution and in particular on the nature of the processes driving the emplacement of the Occator faculae. Gravity science carried throughout the low altitude orbit will be used to resolve the subsurface structure of these large craters.

During its course to the low resonant orbit, Dawn paused at an intermediate orbit with a periapsis close to LAMO to perform observations of the better-illuminated southern polar region with VIR. The objectives of that phase are to map the distribution of the ammonium signature against geological features. Dawn will carry out FC color imaging of high-priority targets in the northern hemisphere to obtain new or repeat coverage. Along with the GRaND results, these data will contribute to the goal of testing hypotheses of Ceres' origin and hydrothermal

evolution, as well as understanding cryomagmatic processes.

Lastly, throughout XM2 Dawn will keep monitoring for solar energetic proton events to be correlated with ground-based telescopic search for outgassing [2] in order to characterize the mechanism(s) of vapor production at Ceres, with applications to other ice-rich bodies.

2. End of Mission

Once the spacecraft runs out of hydrazine, it will lose the ability to maintain the solar arrays pointing to the sun, and the spacecraft will lose power. That time is expected in the early Fall 2018. Dawn will continue to orbit Ceres stably in the eccentric orbit for decades to come in accordance with the planetary protection requirements.

Acknowledgements

A portion of this work was conducted by the Jet Propulsion Laboratory, California Institute of Technology, under contract with NASA.

References

[1] Rayman, M. D.: Dawn at Ceres: The first exploration of the first dwarf planet, 68th International Astronautical Congress, 25-29 September 2017, Adelaide, Australia, Paper IAC-17.A3.4A.2x39024, 2017.

[2] Rousselot, P., et al.: Search for water outgassing of (1) Ceres near its perihelion, This Conference, 2018.

EPSC Abstracts
Vol. 12, EPSC2018-623, 2018
European Planetary Science Congress 2018

Circumferential Fractures around Craters on Ceres and their Implications for the Properties of the Subsurface

K. A. Otto (1), S. Marchi (2), A. J. Trowbridge (3), J. H. Melosh (3), H. G. Sizemore (4)
(1) German Aerospace Center (DLR), Institute for Planetary Research, Berlin, Germany (katharina.otto@dlr.de), (2) Southwest Research Institute, Boulder, CO, USA, (3) Purdue University, Department of Earth, Atmospheric and Planetary Science, Lafayette, IN, USA, (4) Planetary Science Institute, Tucson, Arizona, USA

Abstract

Based on image data from the Dawn Framing Camera (FC), we investigate craters with circumferential fracturing beyond the crater rim on dwarf-planet Ceres. Finite element modeling of a subsurface layer of low viscosity beneath a characteristic crater (50 km diameter) was conducted. The results show that the relaxation of such a subsurface layer introduces stresses that may be responsible for concentric normal faulting around craters on Ceres.

1. Introduction

The Dawn space craft is currently in orbit around the dwarf planet Ceres [1]. Ceres is believed to possess a relatively viscous mantle and mechanically strong crust that contains salts, clathrates, carbonates and ammoniated phyllosilicates [2, 3, 4, 5] together with up to 40 vol % water ice [4]. However, the detailed structure, particularly the properties of the heterogeneity of Ceres' crust [4], is still unknown.

FC images acquired from Low Altitude Mapping Orbit (LAMO; 35 m/px) revealed several relatively young craters on Ceres exhibiting small scale fractures beyond the crater rim that circumferentially surround the crater [6] (Figure 1). These features appear to be unique when compared to other planetary objects with high resolution image data available such as Mars, the Moon or asteroid Vesta. The fracturing may also cause erosion of crater rims to occur more efficiently on Ceres compared to other bodies, potentially explaining the missing large craters on Ceres [7].

Here, we present a possible formation process of the circumferentially fractured craters that leads to possible insights to subsurface material properties and the heterogeneity of Ceres crust.

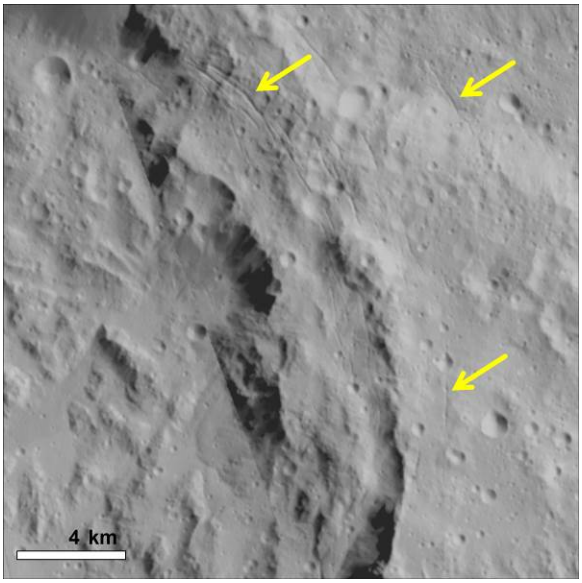

Figure 1: Circumferential fractures around the 50 km diameter crater Ikapati on Ceres. The yellow arrows point at some of the fractures. The crater rim is visible as the curved structure cutting through the image. Some of the fractures are directly on the crater rim, whereas others are located beyond it.

2. Modelling

It is possible that the concentric fractures result from crater relaxation on top of a low viscosity subsurface layer. Similar to observations made at the Canyonlands National Park, Utah [8], the overburden induced deformation of a low viscosity layer allows the surface rocks outside the crater to glide inward toward the crater cavity, opening concentric cracks and/or graben in the terrain immediately surrounding the crater.

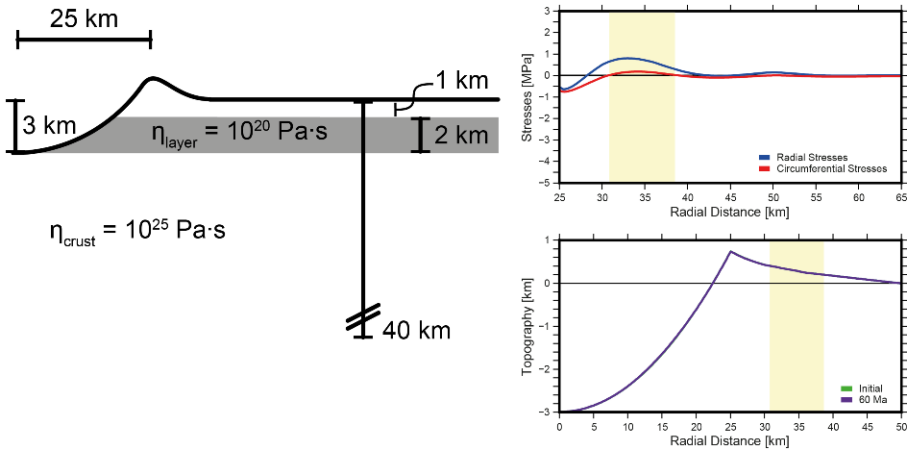

Figure 2: Left: Example of a simulation set-up to explore the effects of a low viscosity layer in Ceres subsurface. Right top: the radial and circumferential stresses that developed around the crater after 60 Ma. Right bottom: The Topography of the simulated crater. The yellow shaded areas on the right hand side mark the position where circumferential fracturing is possible.

Using the the finite element modelling software package Abaqus (Dassault Systèmes), we simulate a 50 km diameter crater with 3 km depth and a parabolic shape. This crater was placed into a 40 km thick and 1287 kg/m^3 dense crust with a viscosity of 10^{25} Pa·s corresponding to the maximum observed viscosity [5]. The crust covers a mantle with a density of 2432 kg/m^3. To estimate the effects of a potential subsurface ice-rich layer, we simulated crater relaxation in the presence of a layer with a viscosity of 10^{20} Pa·s and varying thickness and depth in the shallow crust. Figure 2 shows an example of the simulation geometry and results.

After 60 Ma, simulation set-ups with relatively thin (~2 km thickness) and shallow (~1 km depth) low viscosity layers generate positive radial stresses that exceed the circumferential stresses and thus allow normal faulting (Figure 2).

3. Summary and Conclusions

The concentric fracturing around some crater on Ceres may be a result of a relaxing low viscosity subsurface layer. Finite element modelling suggests that a crater of 50 km diameter may form concentric normal faulting after 60 Ma in the observed location when a low viscosity layer of 2 km thickness is buried 1 km below the surface.

Acknowledgements

We thank the Dawn team for the development, cruise, orbital insertion, and operations of the Dawn spacecraft at Ceres. K.A.O. would like to gratefully acknowledge the financial support and endorsement from the DLR Management Board Young Research Group Leader Program and the Executive Board Member for Space Research and Technology.

References

[1] Russell, C.T., Raymond, C.A., Ammannito, E. et al.: Dawn arrives at Ceres: Exploration of a small, volatile-rich world. Science, 353, 1008–1010,2016. [2] De Sanctis, M.C., Ammannito, E., Raponi, A. et al.: Ammoniated phyllosilicates with a likely outer Solar System origin on (1) Ceres. Nature, 528, 241–244, 2015. [3] De Sanctis, M.C., Raponi, A., Ammannito, E. et al.: Bright carbonate deposits as evidence of aqueous alteration on (1) Ceres. Nature, 536, 54–57, 2016. [4] Bland, M.T., Raymond, C.A., Schenk, P.M. et al.: Composition and structure of the shallow subsurface of Ceres revealed by crater morphology. Nature Geoscience, 9, 538–542, 2016. [5] Fu, R.R., Ermakov, A.I., Marchi, S. et al.: The interior structure of Ceres as revealed by surface topography. Earth and Planetary Science Letters, 476, 153–164, 2017. [6] Buczkowski, D.L., Williams, D.A., Scully, J.E.C. et al.: The geology of the occator quadrangle of dwarf planet Ceres: Floor-fractured craters and other geomorphic evidence of cryomagmatism. Icarus, 1–12, 2017. [7] Marchi, S., Ermakov, A.I., Raymond, C.A. et al.: The missing large impact craters on Ceres. Nature Communications, 7, 1–9, 2016. [8] Walsh, P. and Schultz-Ela, D. D.: Mechanics of graben evolution in Canyonlands National Park, Utah. Geological Society of America Bulletin, 115, 259–270, 2003.

EPSC Abstracts
Vol. 12, EPSC2018-645-1, 2018
European Planetary Science Congress 2018

Dawn Data Reveal Ceres' Complex Crustal Evolution

Carol Raymond (1), Julie Castillo-Rogez (1), Ryan Park (1), Anton Ermakov (1), Michael Bland (2), Simone Marchi (3), Thomas Prettyman (4), Eleonora Ammannito (5), M. Cristina De Sanctis (6), Christopher T. Russell (7)

(1) Jet Propulsion Laboratory, California Institute of Technology, Pasadena, CA, USA; (2) USGS, Flagstaff, AZ, USA; (3) SwRI, Boulder, CO, USA; (4) Planetary Science Institute, Tucson, AZ, USA; (5) ASI, Rome, Italy; (6) IAPS, Rome, Italy; (7) University of California Los Angeles, IGPP/EPSS, Los Angeles, CA, USA. (carol.a.raymond@jpl.nasa.gov)

Abstract

Dawn mapped Ceres using its framing camera (FC), visible and infrared mapping spectrometer (VIR) and gamma-ray and neutron detector (GRaND) during its primary and extended mission, while deriving Ceres' gravity by high-precision navigation data and topography from multi-angle images. These observations show that Ceres' surface has a heterogeneous crater dsitribution, whereas its ammoniated-phyllosilicate rich surface composition is remarkably uniform [1, 2, 3]. Dawn's gravity and topography observations show that Ceres is close to hydrostatic equilibrium and its topography appears to be compensated [4, 5]. However, there are deviations from isostasy that, together with composition and morphological data sets, reveal processes shaping the evolution of Ceres' crust and mantle.

1. Global Interior Structure

Dawn's gravity and topography data are consistent with a partial physical differentiation into a volatile-rich shell (crust) overlying a denser interior of hydrated silicates [4, 5, 6]. Estimates of crustal density and layer thicknesses assuming a two layer model constrained by assuming meteorite grain densities for the hydrated silicate interior range from 1680 kg/m^3 (~70 km thick) to 1900 kg/m^3 (~190 km thick) corresponding to CI (2460 kg/m3) and CM (2900 kg/m3) class meteorites, respectively [4]. Complementary constraint from admittance modeling yields a best-fit crustal density of ~1250 kg/m^3 in a layer ~40 km thick under assumption of Airy isostasy [5], with a corresponding mantle/core density of ~2400 kg/m^3. Preservation of craters <300 km in diameter on Ceres' surface indicate that the outermost layer, here called the crust, is of order 1000x stronger than water ice. A mixture of silicates, salt hydrates and methane clathrates, with no more than ~30% water ice, is consistent with crater morphologies [7], the global topographic power spectrum [6] and the crustal density estimates. However, variability in crater morphology indicates local variability in crustal rheology. While infrared VIR spectra show only a few small patches of water ice, GRaND data show a shallow ice table with ~10% water ice in polar latitudes; water table retreat yields a drier regolith in equatorial latitudes [8]. While the density and thickness of the strong crustal layer is not tightly constrained, a consistent picture has emerged of a layer of mixed ice, silicates and light strong phases best matched by hydrated salts and clathrates, overlying a mantle of hydrated silicates. This partially differentiated interior, combined with the ubiquitous presence of ammoniated phyllosilicates [3] and carbonates [9] on the surface points towards pervasive aqueous alteration. The absence of an ice-dominated layer in the subsurface (from ocean freezing) may indicate partial loss of the ice shell by impact-induced sublimation [10], and mixing with the salts and silicate rich material present near an ancient seafloor.

2. Regional Anomalies

While much of Ceres topography appears to be isostatically compensated, there are significant residual anomalies that likely reflect density variations and/or dynamic processes in the subsurface. The major anomalies at Hanani Planum, Ahuna Mons, and Kerwan crater are discussed by [5], and may indicate emplacement of material of contrasting density into the crustal layer. In addition to these features, there are broad scale correlations between gravity variations, shown as Bouguer and isostatic anomalies, and other surface characteristics. There is a general negative correlation between topography and Bouguer gravity, which is only partially explained by isostatic compensation [4, 5]. One such correlation occurs between the Bouguer gravity and the planitia identified by [11].

Three large shallow basins with degraded rim topography were identified as possible cryptic impact basins, identified as planitiae A-C; Figure 1, top panel shows these planitiae marked on a topographic map. The middle panel shows the Bouguer anomaly field (degrees 3-12) and the bottom panel shows the 3.1-micron band depth [after 12], which indicates lateral variations in the NH_4-phyllosilicate abundance. For planitiae A and C, an enrichment in NH_4 is shown by the light yellow color in the bottom panel. This presents the question of a common process that created the low topography, higher gravity and ammonium enrichment.

3. Implications for Ceres' Evolution

In the context of the global interior structure, the broad-scale regional correlations described above may be explained by impact excavation of the shallow crust, exposing a denser, deeper-seated more ammonium-rich lithology. This interpretation, which is preferred to explain the compositional variations [12], is further strengthened by the gravity-topography correlation, and may provide an explanation for variations in crustal strength and the distribution of volatile-rich deposits on the surface.

Acknowledgements

A portion of this work was conducted by the Jet Propulsion Laboratory, California Institute of Technology, under contract with NASA.

References

[1] Russell C.T. *et al*. (2016) *Science*, *353*, 1008-1010.

[2] Hiesinger H. *et al*. (2016) *Science, 353*, aaf4759-1.

[3] DeSanctis M.C. *et al*. (2015) *Nature, 528,* 241-244.

[4] Park R. *et al*. (2016) *Nature, 537,* 515.

[5] Ermakov A. *et al*. (2017) *JGR Plan*., 122, 2267–2293.

[6] Fu, R. R. et al. (2017) *EPSL, 476*, 153-164.

[7] Bland M.T. *et al*. (2015) *Nat Geosci*, 9, 538-542.

[8] Prettyman T. H. *et al*. (2017) *Science, 355*, 55-59.

[9] DeSanctis M. C. *et al*. (2016) *Nature, 536*, 54.

[10] Castillo-Rogez J. *et al*. (2017) *LPS 48*.

[11] Marchi S. *et al* (2016) *Nat Comm*., 7, 12257.

[12] Ammannito E. *et al*. (2016) *Science, 353*, aaf4279-1.

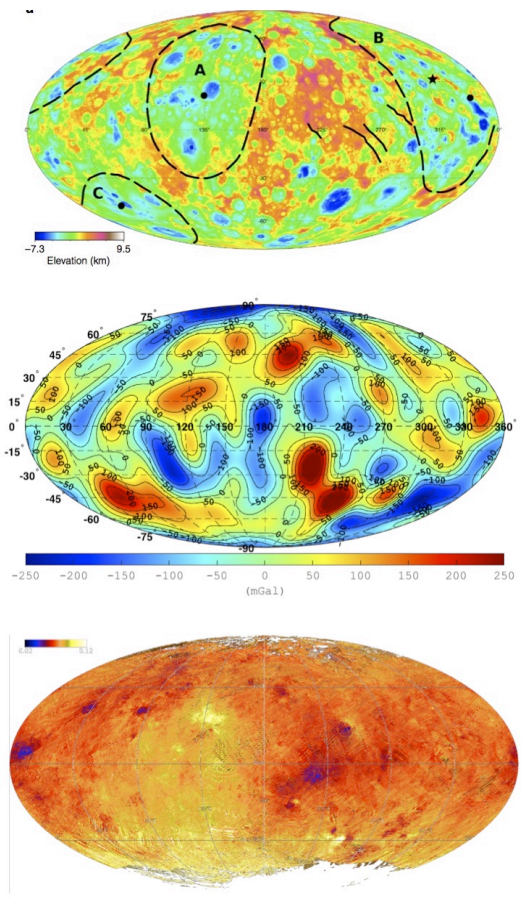

Figure 1. A broad-scale correlation is apparent between topography (and planitiae) shown in top panel from [11], with Bouguer gravity shown in middle panel, and 3.1-micron band depth shown at bottom (after [12]).

EPSC Abstracts
Vol. 12, EPSC2018-651, 2018
European Planetary Science Congress 2018

Unique light scattering at Occator's Faculae on (1) Ceres

A. Nathues (1), M. Hoffmann (1), J. Ripken (1), G. Thangjam (1), T. Platz (1), K. Mengel (2)
(1) Max Planck Institute for Solar System Research, Goettingen, Germany, (nathues@mps.mpg.de), (2) Clausthal Technical University, Clausthal-Zellerfeld, Germany

Abstract

Imagery of the central region of Occator crater obtained by Dawn's Framing Camera is photometrically analysed. The scattering behaviour of the floor faculae is confirmed to be consistent with the appearance of an optically thin near surface haze.

1. Introduction

A prime target of the Dawn mission at Ceres is the Occator crater, hosting the brightest cerean surface features [e.g., 1, 2, 3, 4, 5, 6, 7]. These features populate a portion of its floor and are composed mainly of carbonates, mixed with some dark ammoniated minerals [8]. The bright deposits at Occator's center are significantly younger than the impact crater itself and are likely of cryo-volcanic origin [2, 3]. The dome, located in the central pit, is possibly the outcome of a long lasting, periodic or episodic ascent of bright material from a subsurface brine reservoir. Originally triggered by an impact event, gases, possibly exsolved from a subsurface brine reservoir, enabled the bright material to ascend through fractures and deposited onto the surface [2, 3].

During Rotational Characterization 3 (RC3) orbit the Framing Camera (FC) obtained low spatial resolution images (~1.3 km/pix) of Ceres. This imagery led to the detection of an unusual light scattering behavior at the floor of Occator, which was attributed to a diurnal varying near surface haze [1], which was later on confirmed and detailed by [9]. However, [10] argued that there are no evidences for haze. We revisited the reported effect by [1] and [9] by using RC3 and more recent data from RC4 and CXO mission phases, which have been obtained at favorable observation geometries.

2. Results

We computed reflectance ratios between individual bright material sites belonging to the Occator faculae and nearby (dark) floor sites in order to identify differences in their reflectance behavior versus geometry. Figure 1 displays the ratio between one of the investigated site combinations versus cos *e* for three different mission phases. In all three data sets, the ratio max/median is a positive sloped function, i.e. with decreasing *e* the ratio increases. This effect is seen in each data set but different in degree of correlation. For each of the RC and CXO sets the phase angle kept virtually constant, and is not responsible for the trends in Fig. 1.

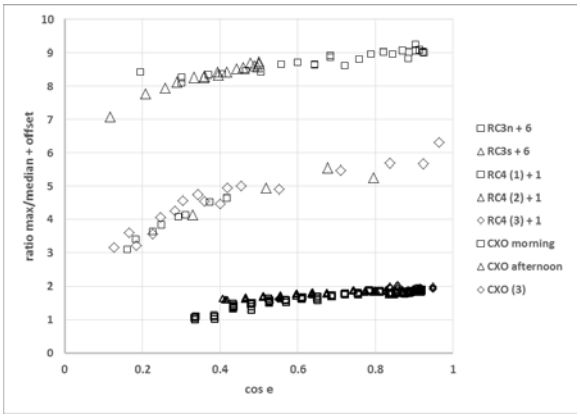

Fig. 1: *Reflectance ratio between a bright and a dark material site within Occator versus cos e. Results from three different mission phases (RC3, RC4 and CXO) are shown. RC3 and RC4 data has been offset for clarity. The reflectance ratio increases with cos e. Statistical errors are on the order of symbol size.*

In order to investigate whether the light scattering behavior of Occator's faculae is indeed unique or found elsewhere, we measured bright and dark sites at other localities for comparison. By contrast with the Occator findings, all ratios of reference sites exhibit approximately constant levels in reflectance after applying a global photometric correction; none is showing such a strong correlation with emission angle or a diurnal variation of reflectance. Approximately constant ratio levels for varying emission and incidence angles indicate that the light scattering behavior of bright and dark units outside Occator's floor are similar, i.e. these sites have

similar light scattering parameters than the global surface.

3. Discussion

[1] and [9] reported, based on RC3 data, a diurnally variable enhancement of light excess near the centre of the Occator crater, which was attributed to an optically thin haze. Our current work, using multiple datasets from different mission phases, obtained under different observation geometries, confirms the unique light scattering characteristic of Occator's faculae.

In order to discard or confirm the haze hypothesis two further potential explanations need to be discussed: 1) The unique light scattering being a result of a spatial resolution effect of a scene, which is optically shortened while moving towards the limb; and 2) The effect is a result of differential light scattering parameters of different planetary surface materials. We found that the potential explanations 1) and 2) are highly unlikely compared to the haze hypothesis since only the latter hypothesis allows us to explain the fact that the reflectance ratio of a faculae varies with emission angle while the phase angle is constant in the absence of shadows.

4. Summary and Conclusions

A thorough comparison of reflectance data from different mission phases resulted in a further confirmation of a light excess measured in the central region of Occator. This excess is unlikely to be caused by a unique facuale material. Although the available data sets do not allow a determination of all necessary free parameters, which are required to develop a unique quantitative model, a consistent qualitative explanation for the phenomenon in terms of an optically thin haze has been identified. Several different locations on Ceres with contrasts of reflectance do not follow similar dependencies. Thus, Occator as an outstanding location on Ceres is further manifested.

References

[1] Nathues et al. 2015, Sublimation in bright spots on (1) Ceres, Nature 528

[2] Nathues et al. 2017, Evolution of Occator Crater on (1) Ceres. The Astronomical Journal, Vol. 153, pp. 112–124.

[3] Nathues et al. 2018, Occator crater in color at highest spatial resolution. Icarus, in press.

[4] Ruesch et al. 2018, Bright carbonate surfaces on Ceres as remnants of salt-rich water fountains. Icarus, in press.

[5] Stein et al. 2018, The formation and evolution of bright spots on Ceres. Icarus, in press.

[6] Quick et al. 2018, A Possible Brine Reservoir Beneath Occator Crater: Thermal and Compositional Evolution and Formation of the Cerealia Dome and Vinalia Faculae, Icarus, in review

[7] Scully et al. 2018, Introduction to the special issue: The formation and evolution of Ceres' Occator crater, Icarus, in press

[8] De Sanctis et al. 2016, Bright carbonate deposits as evidence of aqueous alteration on (1) Ceres. Nature volume 536, pages 54–57.

[9] Thangjam et al. 2016, Haze at Occator Crater on Dwarf Planet Ceres, Astrophysical Journal Letters, Volume 833, Number 2.

[10] Schröder et al. 2017, Resolved spectrophotometric properties of the Ceres surface from Dawn Framing Camera images, Icarus, Volume 288, Pages 201-225.

EPSC Abstracts
Vol. 12, EPSC2018-685, 2018
European Planetary Science Congress 2018

IR spectroscopy of ammoniated phyllosilicates at low pressure/high temperature conditions

S. De Angelis (1), M. Ferrari (1), M.C. De Sanctis (1), E. Ammannito (2)
(1) Institute for Space Astrophysics and Planetology, IAPS-INAF, Rome Italy, (simone.deangelis@iaps.inaf.it) (2) Italian Space Agency – ASI, Rome, Italy

Introduction

Ammonium phyllosilicates are thought to be among the constituents of dwarf planet (1) Ceres surface, based on ground-based telescopic [1] and VIR-Dawn spectral data [2]. Following these findings, several works are currently trying to reproduce in the laboratory the Ceres surface composition, in terms of multi-component mineral mixtures [3,4]. Thus it is of interest to investigate the behavior and stability of ammonium compounds, when measured at pressure-temperature conditions that are different from standard laboratory values. Here we describe Visible-Infrared spectroscopic measurements of an ensemble of ammonium phyllosilicates: spectra have been acquired at various pressure-temperature conditions, by means of a P-T cell realized at INAF-IAPS laboratory.

1. Samples and experimental setup

Ammoniated phyllosilicates were produced in the laboratory starting from natural samples, following a procedure described in a series of works [e.g. 6].
Infrared spectra of five ammoniated samples (montmorillonite, SCa-3, two nontronites, NAu-1 and NAu-2, illite-smectite, ISCz-1 and hectorite, SHCa-1) were then acquired in the spectral range 0.35-2.5 μm, by using an ASD FieldSpec Pro 4 spectro-photometer equipped with a QTH lamp. The instrument is characterized by a spectral resolution of about 3-10 nm in the whole range; the spatial resolution of the setup was about 5 mm on the sample. All samples were analyzed in the form of powder, with grain size d<36 μm.
In order to acquire reflectance spectra at varying conditions, the samples were placed inside a P-T environmental cell, developed at INAF-IAPS [5]. The measurements strategy was the following: (i) acquisition at room P-T, (ii) sequence of acquisitions at room T during pumping; in this stage the pumping was first performed with only primary diaphragm pump (down to a limit of 3-4 mbar) and then also with turbo-molecular pump (down to vacuum pressure of 10^{-4}-10^{-5} mbar); (iii) acquisitions in vacuum at higher temperatures.

2. IR Spectral measurements.

Here we report, as an example, on the analyses performed on one sample, nontronite (NAu1). The spectra of NH_4-Nontronite are shown in fig.1. Data were acquired in three stages. The first spectrum (fig.1, A) is at room pressure and temperature. In panel B spectra were acquired at room T during primary pumping from ambient to 10^{-4} mbar. Finally in panel C spectra acquired in vacuum at different temperatures (50-240°C) are shown.

3. Results and Conclusions

Spectra of nontronite are characterized by Fe^{2+}-Fe^{3+} bands at 0.7-1 μm, and by OH^-/H_2O bands at 1.4 and 1.9 μm [7]. The feature at 2.3 μm is Fe-OH [7]. NH_4^+ absorption is visible at 2.12 μm in the room P-T spectrum. After pumping the adsorbed water is removed and NH_4^+ features become evident also at 1.55 and 2.01 μm: at room P-T these two features are shoulders in the 1.4 and 1.9 μm bands. After heating up to 240°C all NH_4^+ bands are visible and quite separate from hydration bands.
We can see that NH_4^+ bands remain quite unaltered both by the process of pumping, at least down to a vacuum of about 10^{-4} mbar, and by the process of heating up to 240°C. For higher temperatures the nontronite sample is subject to structural changes: all the water is removed, then ammonia and finally dehydroxylation occurs (fig. 1C).

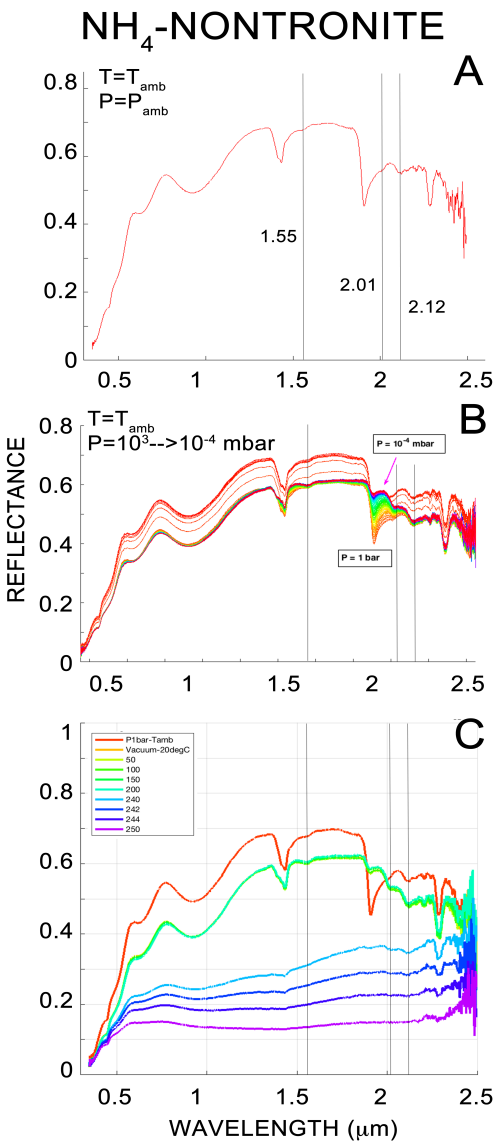

Fig.1. NH_4-Nontronite (NAu-1). A): ambient pressure and temperature; B): ambient temperature, during pumping; C): higher temperatures, in vacuum. Vertical lines indicate NH_4^+ absorptions.

Acknowledgements

The experiment is funded by ASI.

References

[1] King T.V.V. et al., Science, vol.255, 1551-1553, 1992
[2] De Sanctis M.C., et al., Nature, vol.528, 241-244, 2015.
[3] De Angelis S. et al., EPSC abstract n.830, vol.11, 2017
[4] Ehlmann B.L. et al., MAPS, 10.1111/maps.13103, 2018
[5] De Angelis S. et al., 49th LPSC, abstract n.1428, 2018
[6] Ferrari M. et al., 49th LPSC, abstract n.2413, 2018
[7] Clark R.N. et al., JGR, vol.95, B8, 12,653-12,680, 1990

EPSC Abstracts
Vol. 12, EPSC2018-710, 2018
European Planetary Science Congress 2018

Basaltic asteroids observed with ESO/XShooter

A. Migliorini (1), M.C. De Sanctis (1), D. Lazzaro (2), M. Barbieri (3), D. Mesa (3), M. Lazzarin (4)

(1) IAPS-INAF, Rome, Italy, (2) Observatorio Nacional, Rio de Janeiro, Brazil, (3) University of Atacama, Copiapo, Chile, (4) Università degli Studi di Padova, Padova, Italy, (email: alessandra.migliorini@iaps.inaf.it)

1. Introduction

We present new spectroscopic observations of 17 putative basaltic asteroids, in the 0.3-2.5 μm region, with the ESO/XShooter facility. The observed spectral range encompasses the two pyroxene bands centred at 0.9 and 2.0 μm, typical of the basaltic asteroids. The data allowed to taxonomically classify the observed asteroids, and in some cases to confirm their basaltic nature.

2. Data selection and reduction

Observations were carried out at ESO/VLT, equipped with the XShooter spectrograph (Vernet et al. 2011), on 13-14 October 2017 (program ID 0100.C-0698(A)). This instrument allows covering the wavelength region 0.3-2.5 μm in a single acquisition.

Asteroids were selected from lists of putative basaltic asteroids, compiled on the basis of visible (Roig et al. 2006) and near-infrared (Licandro et al. 2017) colors. Putative basaltic candidates, distributed throughout the Main Belt regions, were identified and observed, aiming to compare properties of asteroids belonging to the Vesta family and located outside the family region. In particular, 8 asteroids out of the 17 are located in the Middle region and 4 in the Outer region of the Main Belt. Observational details are provided in table 1.

Data were calibrated using the ESO pipeline REFLEX (Freudling et al. 2013), which includes bias correction, flat-fielding and wavelength calibration. Asteroids were finally divided by solar analogs, to obtain the relative reflectance.

3. Results

Most of the observed asteroids present the two absorption bands at 0.9 and 2.0 μm. However, most of the asteroids located in the middle and outer main belt regions show slightly different pyroxenes bands with respect the typical basaltic absorption bands. Hence, the preliminary taxonomic classification, using the Demeo online tool (Demeo et al. 2009), for most of these asteroids is more close to S and X complex. On the other hand, the basaltic nature is clearly confirmed only for 4 objects, of which only one located in the Outer belt.

Table 1. Observing circumstances.

Asteroid	Semimajor axis (AU)	Inclination (°)
2452	3.157	8.98
5758	2.247	0.58
7675	2.414	7.51
9197	2.163	2.46
10800	2.549	5.30
17239	3.046	2.65
22308	2.773	6.46
36118	2.709	4.25
48797	2.939	3.69
66905	2.746	8.39
67299	2.575	15.6
73076	1.961	21.2
76551	2.373	7.05
85812	2.844	10.2
93580	2.644	16.6
93620	2.632	8.27
189597	2.658	11.1

For the confirmed basaltic asteroids, the acquired spectra have been analysed in order to derive compositional surface information. Comparison with

previously acquired V-type asteroids spectra will also be presented.

The acquired data allow to have a better insight on the selection parameters for putative basaltic asteroids and to provide further progress in the basaltic material distribution throughout the Solar System.

Based on observations made with the VLT/Xshooter of the European Southern Observatory, under ESO program 0100.C-0698(A).
DL was supported by diverse grants and fellowships by FAPERJ and CNPQ.

References

[1] DeMeo F.E., Binzel R.P., Slivan S.M., Bus S.J., 2009, Icarus, 202, 160.

[2] Freudling W. et al., 2013, Astron. Astrophys., 559, A96.

[3] Licandro J., Popescu M., Morate D., de Léon J., A&A, 600, A126.

[4] Roig F. and Gil-Hutton R., 2006, Icarus, 183, 411.

[5] Vernet et al. 2011, A&A, 536A, 105.

EPSC Abstracts
Vol. 12, EPSC2018-751, 2018
European Planetary Science Congress 2018

Disk-resolved photometry of Vesta and Ceres

A. Longobardo (1,2), E. Palomba (1,3), M.C. De Sanctis (1), M. Ciarniello (1), A. Galiano (1,4), S.E. Schroeder (5), E. Ammannito (6), F. Tosi (1), F. Capaccioni (1), F. Zambon (1), F.G. Carrozzo (1), A. Raponi (1), M.T. Capria (1), K. Stephan (5), E. Rognini (1), C.A. Raymond (7), C.T. Russell (8)
(1) INAF-IAPS, via Fosso del Cavaliere 100, 00133 Rome, Italy (andrea.longobardo@iaps.inaf.it); (2) DIST, Università Parthenope, Naples, Italy; (3) ASI-SSDC, Rome, Italy; (4) Università Tor Vergata, Rome, Italy; (5) DLR, Belin, Germany; (6) ASI-URS, Rome, Italy; (7) JPL, Pasadena, CA, USA; (8) UCLA, Los Angeles, CA, USA

Abstract

We summarize the results obtained by the VIR spectrometer on board the NASA/Dawn mission about photometry of Vesta and Ceres. Phase functions and photometric behavior of absorption bands are mainly affected by optical properties, but in localized regions an important role is also played by surface roughness.

1. Introduction

The NASA/Dawn mission [1] orbited Vesta and is still orbiting Ceres, and hyperspectral images of the two bodies were acquired by means of the Visible and InfraRed (VIR) mapping spectrometer [2].
VIR confirmed Vesta as parent body of the HED achondrite clan [3]. The Vesta spectra are characterized by two deep absorption bands, due to pyroxene and centred at about 1 μm and 2 μm. Vesta is the asteroid with the largest albedo variation on its surface, because of the occurrence of carbonaceous chondrites [4], which darken the surface and makes the pyroxene bands shallower in several locations [5].
Ceres is a C-type asteroid, and its spectra are characterized by reflectance absorption at 2.7 μm (phyllosilicates), 3.1 μm (ammonium), 3.4 μm (ammonium and carbonates) and 3.9 μm (carbonates) [6,7]. Whereas Ceres is an overall dark body (I/F~0.03 at 0.55 μm and 30° phase), it shows two localized regions, i.e. the Occator faculae, having an albedo up to seven times higher than the Ceres average. They are the result of aqueous alteration, and show a larger abundance of phyllosilicates and especially carbonates, as revealed by the larger depth of the corresponding absorption bands.
We studied the photometric behavior, i.e. trend with incidence, emission and phase angle, of the spectral parameters describing the Vesta and Ceres spectra. This study is not only fundamental for data reduction (because leads all the observations to the same observation geometry), but also gives insights about physical and optical properties of the surface regolith.

2. Method

The method consists in a statistical analysis of the VIR dataset [8, 9, 10], and applies in the following steps: 1) retrieval and application of the disk function, among those defined in literature, which best removes the influence of incidence and emission angle on reflectance; 2) definition of reflectance families, where each family is given by the xx% (with xx=10, 20 … 80, 90) of largest reflectance value measured at each phase angle bin of width 1°; 3) for each reflectance family, retrieval of the function which best fit the behavior of reflectance, band depths and spectral slopes as a function of phase angle; 4) correction, i.e. retrieval of the value at a defined phase angle (0° or 30°).
To better describe the reflectance vs phase angle curve (phase function) we defined two parameters: R30, i.e. the retrieved reflectance at 30° phase angle, and PCS (Phase Curve Slope), i.e. the steepness of the phase function between 20° and 60° phase angle. These parameters were compared with those obtained on other asteroids explored by space missions.

3. Results

Vesta. Visible and infrared reflectance phase function is flatter in the bright terrains and steeper in the darker ones (Figure 1). This was ascribed to the more important role in bright terrains of multiple scattering, which redistribute the incident radiation at all the phase angles. For the same reason, the deepening of the pyroxene bands at increasing phase angle is more evident in dark terrains and almost absent in the bright ones. The photometric behaviour of the two band depths is similar, in agreement to the fact that their carrier is the same. Finally, a dependence of band centers on incidence angle was observed, in

agreement with the HED band center dependence on temperature measured in laboratory experiments [11].

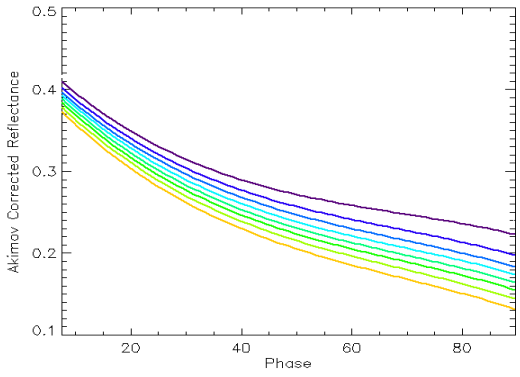

Figure 1. Phase functions corresponding to different Vesta's reflectance families. Cold (hot) colors correspond to bright (dark) terrains.

Ceres. Ceres is much more homogeneous than Vesta in terms of albedo, and its photometric properties are also constant across its surface, except in the Occator's faculae. Whereas the high steepness of the Ceres phase function of Ceres is justified by its low albedo, the high PCS of the Occator's faculae cannot be justified by optical properties only (PCS of asteroids having the same R30 of Occator is much lower, see Figure 2). It is therefore possible that the high roughness of this region [12] affects its photometric properties. For the Ceres average, all the band depths and the spectral slope increase with phase, as expected. The only exception is the 3.9 μm band depth, generated by a bright carrier (carbonates) and hence independent of phase. For the Occator's faculae, the 2.7 μm band depth decrease with phase is two times larger, while 3.4 and 3.9 μm are both phase-independent. The first behaviour can be explained again with the highest roughness of the faculae region. The second one is instead due to the fact that in this region the 3.4 μm absorption is due almost exclusively to carbonates (contrarily to the Ceres average) and hence has the same photometric behaviour of the 3.9 μm band depth. Spectral slope is also phase-independent on Occator, and this could be explained with absence of phase reddening for carbonates.

4. Conclusions

Disk-resolved photometry of Vesta and Ceres (and, more generally, of other asteroids) is mainly driven from optical properties, i.e. albedo and role of multiple/single scattering. The R30-PCS combination is a tool to discriminate different taxonomic classes. In addition, mixtures between two taxonomic types (e.g., the Vesta dark terrains consist in a HED-CC mixture) show intermediate photometric parameters between the classes.

However, we have found at least one location (the Occator's faculae on Ceres) where physical properties, specifically the surface roughness, also strongly affect the photometry.

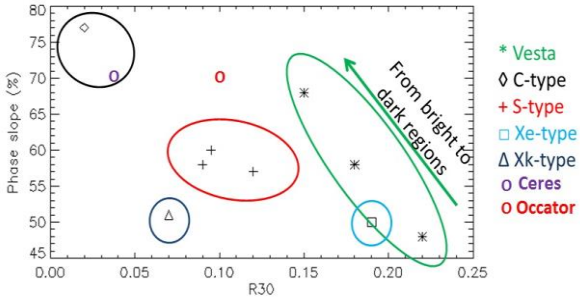

Figure 2: R30 vs PCS scatterplot for Vesta's dark, intermediate and bright terrains, Ceres average, Occator's faculae and other asteroids [9].

Acknowledgements

VIR is funded by the Italian Space Agency–ASI and was developed under the leadership of INAF-Istituto di Astrofisica e Planetologia Spaziali, Rome-Italy. The instrument was built by Selex-Galileo, Florence-Italy. The authors acknowledge the support of the Dawn Science, Instrument, and Operations Teams.

References

[1] Russell, C.T., et al. (2011). Springer, ISBN: 978-1-4614-4902-7; [2] De Sanctis, M.C. et al. (2011), SSR 163, 329-369; [3] De Sanctis, M.C. et al. (2012), Science 336, 697-700; [4] McCord, T.B. et al. (2012), Nature 491, 83-86; [5] Palomba, E. et al. (2014), Icarus 240, 58-73; [6] De Sanctis, M.C. et al. (2015), Nature, doi:10.1038/nature16172; [7] De Sanctis, M.C. et al. (2016), Nature, doi:10.1038/nature18290; [8] Longobardo, A. et al. (2014), Icarus 240, 20-35; [9] Longobardo, A. et al. (2016), Icarus 267, 204-216; [10] Longobardo, A. et al. (2018), doi: 10.1016/j.icarus.2018.02.022; [11] Burbine, T.H. et al. (2011), MAPS, 44, 9, 1331-1341; [12] Buczkowski, D.H. et al. (2017), Icarus in press. doi: 10.1016/j.icarus.2017.05.025

EPSC Abstracts
Vol. 12, EPSC2018-757, 2018
European Planetary Science Congress 2018

Basaltic material in the main belt: a tale of two parent bodies?

S. Ieva (1), E. Dotto (1), D. Lazzaro (2), D. Fulvio (3), D. Perna (1,4), E. Mazzotta Epifani (1), H. Medeiros (2), M. Fulchignoni (4)
(1) INAF – Osservatorio Astronomico di Roma, Via Frascati 33, 00078 Monte Porzio Catone (Roma), Italy (simone.ieva@oa-roma.inaf.it)
(2) Observatório Nacional, R. Gal. José Cristino 77, 20921-400 Rio de Janeiro, Brazil
(3) Departamento de Física, Pontifícia Universidade Católica do Rio de Janeiro, Rua Marquês de São Vicente 225, 22451-900 Rio de Janeiro, RJ, Brazil
(4) LESIA, Observatoire de Paris, PSL Research University, CNRS, Univ. Paris Diderot, Sorbonne Paris Cité, UPMC Univ., Paris 06, Sorbonne Université, 5 Place J. Janssen, Meudon Cedex F-92195, France

Abstract

The majority of basaltic objects in the main belt are dynamically connected to Vesta, the largest differentiated asteroid known. Others, due to their current orbital parameters, cannot be easily linked to Vesta and could be fragments of another differentiated asteroid. We conducted an on-going spectroscopic survey to characterize basaltic candidates in the middle and outer main belt. Here we present the latest results.

1. Introduction

The study of basaltic asteroids in the main belt has been a powerful tool to constrain the presence and frequency of differentiated material in the early Solar System. These asteroids, classified as V-type in all the latest taxonomies [6], are thought to represent the crust of planetesimals that undergone a complete metal-silicate differentiation: iron core, olivine mantle and basaltic crust.
Vesta has been long considered the parent body for all the basaltic material in the solar system, due to several clues: i) the similarity of their spectrum characterized by two deep absorption bands at 0.9 and 1.9 μm [1,5]; ii) the presence of two large basins in the southern hemisphere of Vesta [12] identified as the origin for the dynamical family (the so-called *vestoids*).
The discovery of V-type asteroids with no dynamical link with Vesta, beyond the 3:1 mean motion resonance with Jupiter [2,7,9] raised doubts if all the basaltic asteroids in the Solar System come from Vesta. Dynamical simulations show that the probability for an asteroid of a D > 5 km to evolve from the Vesta family and cross over the 3:1 resonance, reaching a stable orbit in the middle belt, is almost 1% [11]. Moreover, laboratory studies on meteorites [3,13] and dynamical considerations [4] suggest that several large asteroids (D = 150-300 km) should have been differentiated in the early Solar System. The inconclusive search of these bodies lead to the idea that these basaltic progenitors were battered to bits; or that maybe our understanding of differentiation processes is not complete [10].
In order to characterize basaltic candidates in the middle/outer main belt (or MOVs) we are conducting an observational campaign via visible and near-infrared spectroscopy. The observed objects were identified among the SDSS - Moving Object Catalog (MOC), assuming that candidates with photometric colors and albedo indicative of a basaltic composition are indeed basaltic asteroids.

2. Results

Here we present the latest results of two observational campaigns we have conducted at Telescopio Nazionale Galileo (TNG) in 2015 and at ESO - New Technology Telescope (NTT) in 2016. We spectroscopically characterized 18 MOV candidates in the visible range. In order to compare the results with our previous statistical analysis on the largest collection of V-type spectra [8], we computed three spectral parameters: reflectivity gradients between 0.5-0.75 μm (slopeA) and 0.8-0.92 μm (slopeB) and the reflectance ratio 0.75/0.9 μm (depth). Our analysis has shown that the differences between MOVs and vestoids seem to be more evident comparing slopeB and depth, with the MOV population having the extreme spectral parameters of the sample. Moreover, the analysis of the spectral parameters in three different regions of the main belt with a high concentration of MOVs has shown that the depth is always higher than the Vesta family.

The presence of a cluster of basaltic objects with similar spectral parameters, but different from Vesta's, could be a strong indicator of the presence of another differentiated family. This could alter the current paradigma of differentiation processes, implying that the extension of the temperature gradient in the protosolar nebula at the epoch of planetary formation was different from always thought, in order to reach the right amount of heat able to sustain differentiation at solar distances a > 2.5 au.

Acknowledgements

Support by CNPq (305409/2016-6) and FAPERJ (E-26/201.213/2014) is acknowledged by DL. DF thanks the Brazilian foundation CNPq for financial support (Bolsa de Produtividade em Pesquisa, PQ 2015" - Processo: 309964/2015-6 - and Chamada Universal 2016" - Processo: 426929/2016-0). DP has received funding from the European Union's Horizon 2020 research and innovation programme under the Marie Sklodowska-Curie grant agreement n. 664931.

References

[1] Binzel R. P., Xu S., 1993, Science, 260, 186
[2] Binzel R. P., Masi G., Foglia S., 2006, in AAS/Division for Planetary Sciences Meeting Abstracts #38. p. 627
[3] Bland P. A., et al., 2009, Science, 325, 1525
[4] Carruba V., Huaman M. E., Domingos R. C., Santos C. R. D., Souami D., 2014, MNRAS, 439, 3168
[5] Cruikshank D. P., Tholen D. J., Bell J. F., Hartmann W. K., Brown R. H., 1991, Icarus, 89, 1
[6] DeMeo F. E., Binzel R. P., Slivan S. M., Bus S. J., 2009, Icarus, 202, 160
[7] Duffard R., Roig F., 2009, Planet. Space Sci., 57, 229
[8] Ieva, S., Dotto, E., Lazzaro, D. et al., MNRAS, 455, 2871, 2016
[9] Lazzaro, D., Michtchenko, T., Carvano, J. M. et al. Science, 288, 2033, 2000
[10] Lazzaro D., 2009, in Revista Mexicana de Astronomia y Astro_sica Conference Series. pp 1-6
[11] Roig F., Nesvorn_y D., Gil-Hutton R., Lazzaro D., 2008, Icarus, 194, 125
[12] Russell, C. T., Raymond, C. A., Coradini, A. et al. Science, 336, 684, 2012
[13] Scott, E. R. D., Greenwood, R. C., Franchi, I. A., Sanders, I. S.Geochim. Cosmochim. Acta, 73, 5835, 2009

EPSC Abstracts
Vol. 12, EPSC2018-806, 2018
European Planetary Science Congress 2018

Spectral analysis of Ceres subsurface

A. Galiano (1,2), E. Palomba (1,3), A. Longobardo (1,4), M.C. De Sanctis (1), F.G. Carrozzo (1), A. Raponi (1), F. Tosi (1), E. Ammannito (5), E. A. Cloutis (6) C.A. Raymond (7), C.T. Russell (8) and the VIR team.
(1) INAF-IAPS, Rome, Italy (anna.galiano@iaps.inaf.it), (2) Università degli Studi di Roma Tor Vergata, Rome, Italy, (3) ASDC-ASI, Rome, Italy, (4) Università Parthenope, Naples, Italy (5) ASI-URS, Rome, Italy, (6) Department of Geography, University of Winnipeg, Winnipeg, Manitoba R3B 2E9, Canada (7) JPL, California Institute of Technology, Pasadena, CA, USA, (8) UCLA, Los Angeles, CA, USA.

Abstract

The dwarf planet Ceres is a heavily cratered rocky body and complex craters with a central peak are present on its surface. The material composing the central peaks is the geological unit termed *crater central peak material* (ccp) and corresponds to subsurface rock emergent as consequence of significant impact event. Mineralogical investigation of Ceres subsurface (within a depth of about 22 km) was performed by means of spectral data of 32 ccps, acquired by VIR spectrometer onboard the NASA Dawn spacecraft. Mg-phyllosilicates, NH_4-phyllosilicates and Mg/Ca-carbonates compose both the Ceres subsurface and surface, but their abundances in ccps vary with latitude and depth of excavation.

1. Introduction

The NASA Dawn mission has explored the dwarf planet Ceres since March 2015 and the mineralogical composition of Ceres surface has been obtained by means of spectral data acquired by the Visible and Infrared Mapping Spectrometer (VIR): absorption bands at 2.7-, 3.1-, 3.4- and 4.0-µm in reflectance spectra revealed a surface composition made of Mg-phyllosilicates, NH_4-phyllosilicates, Mg/Ca-carbonates and a dark featureless component, which reduces the albedo [1]. Na-carbonates have been detected in Occator'sfFaculae [2] and in other localized areas of Ceres, such as in the ejecta and floors of Kupalo and Haulani crater [3]. Organics occur on the peak, floor and ejecta of Ernutet crater, as detected by the prominent 3.4-µm absorption band, connected to the C-H bonds of aliphatic organic compounds [4].
To investigate the mineralogical composition of Ceres subsurface we examined the spectral properties of the geologic unit identified as *crater central peak material* (ccp) [5], subsurface rocks exhumed during the formation of large impact craters [6].

2. VIR data

The Dawn spacecraft performed mapping orbits with decreasing altitude from the Ceres surface and VIR spectrometer acquired reflectance spectra in the 0.25-5.1 µm spectral range with increasing spatial resolution. In particular, in the HAMO (High-Altitude Mapping Orbit) phase the spacecraft was at an altitude of 1470 km and VIR acquired spectra with a spatial resolution of 360-400 m/pixel; during the LAMO (Low-Altitude Mapping Orbit) phase the minimum altitude of 385 km was reached and spectral data were acquired with a spatial resolution of 90-110 m/pixel. Data from these two orbital stages were used for this work.

3. Data selection and parameters

Central peaks of complex craters identified from the geological maps of Ceres [5] and observed by VIR data with high spatial resolution, i.e. acquired during the HAMO and LAMO phase, were selected. In total, 32 ccps were analysed, by defining a square-shaped area around each peak. For each ccp, mean values of 2.7-, 3.1-, 3.4- and 4.0-µm band depths and band centers were computed [7], as well as spectral slope estimated between 1.2 and 1.9 µm. Furthermore, the elevation of each crater's peak with respect to the ellipsoidal shape model of Ceres was retrieved and we estimated the subsurface depth from where ccp originated, by subtracting from the maximum elevation a tenth of crater's diameter containing the peak [8].

4. Spectral investigation of ccps

According to our results, the mineralogical composition of the Ceres subsurface reflects the surface, i.e. a mixture of Mg/Ca-carbonates, NH_4-phyllosilicates, Mg-phyllosilicates and a dark component, but particular trend is observed with

higher latitudes and with increasing depth of excavation. For ccps, the 2.7- and 3.1-µm band depths correlate, as observed for the entire Ceres surface [9], i.e. Mg-phyllosilicates and NH_4-phyllosilicates are strongly correlated for the subsurface materials. Furthermore, the abundance of Mg-phyllosilicates and NH_4-phyllosilicates increases in poleward subsurface deposits, as shown in Figure 1. This trend can be due to the fact that the OH group (responsible for the 2.7-µm band) and ammonium-bearing clays (responsible for the 3.1-µm band) are more prominent.

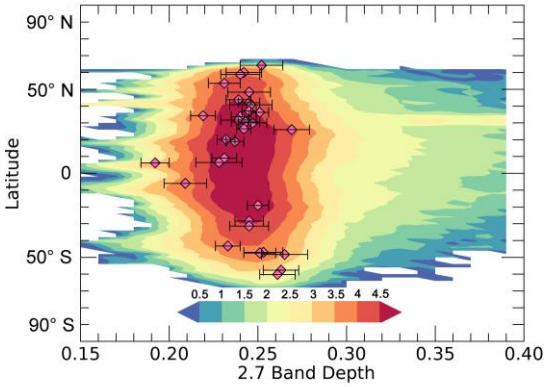

Figure 1: Scatterplot of 2.7 µm band depth of ccps as a function of latitude (magenta diamonds) superimposed on the density plot representing the Ceres surface. Differently from the behavior of Ceres surface, band depths of ccps are stronger at higher latitudes. The Color bar refers to the density of pixels forming the density plot, expressed in logarithmic form, where lower values are represented by blue color and higher values by red color.

The 3.4- and 4.0-µm bands, associated with carbonates, show different trends when compared with the other parameters: the 4.0-µm spectral feature is weakly correlated with 3.1-µm band, while the 3.4-µm band is strongly correlated with spectral features diagnostic of NH_4-phyllosilicates. The 3.4-µm band depth increases at poleward latitudes (as do the 2.7- and 3.1-µm bands, which are features diagnostic of phyllosilicates) while the 4.0-µm band does not show any significant latitudinal trend.

The 3.1- and 3.4-µm band depths show an increase at increasing depth of excavation and show a strong correlation (Figure 2); the 2.7- and 4.0-µm band depths are weakly correlated with excavation depth. This mean that NH_4-phyllosilicates seem to be more concentrated in ccps excavated from greater depth. The 3.4-µm band depth shows a similar trend to the phyllosilicates' bands and in particular to the 3.1-µm band (associated to ammoniated phyllosilicates): in fact, such a spectral feature is not only due to carbonates, but NH_4-phyllosilicates and organics also contribute or affect to its shape and strength.

Furthermore, 3 ccps, i.e. Haulani, Ikapati and Ernutet are composed of Na-carbonates and Mg/Ca-carbonates, in addition to phyllosilicates and dark material, exhumed from a depth of about 6-9 km.

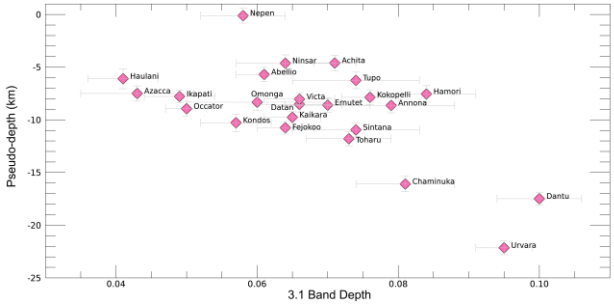

Figure 2: Scatterplot of 3.1 µm band depth of ccps as a function of excavation depth (magenta diamonds).

Acknowledgements

VIR is funded by the Italian Space Agency–ASI and was developed under the leadership of INAF-Istituto di Astrofisica e Planetologia Spaziali, Rome-Italy. The instrument was built by Selex-Galileo, Florence-Italy. The authors acknowledge the support of the Dawn Science, Instrument, and Operations Teams.

References

[1] De Sanctis, M.C. et al., Nature, Vol. 528, pp. 241-244, 2015.

[2] De Sanctis, M.C. et al., Nature, Vol. 536, pp. 54-57, 2016.

[3] Carrozzo, F.G. et al, Science Advances, Vol. 4, Nr. 3, doi:10.1126/sciadv.1701645.

[4] De Sanctis, M.C. et al., Science, Vol. 355, Issue 6326, pp. 719-722, 2017.

[5] Mest, S.C. et al., 49th LPSC Abstract, 2018.

[6] Grieve, R.A.F. et al., Proceeding of the Lunar and Planetary Science 12A (P.H. Schultz and R.B. Merrill eds.), pp. 37-57, Pergamon, New York.

[7] Galiano, A. et al., Advances in Space Research, in press, https://doi.org/10.1016/j.asr.2017.10.039, 2018.

[8] Pan, C. et al., Journal of Geophysical Research: Planets, Vol. 120, pp. 662-688, 2015.

[9] Ammannito, E. et al., Science, Vol. 353, Issue 6303, aaf4279, 2016.

EPSC Abstracts
Vol. 12, EPSC2018-841, 2018
European Planetary Science Congress 2018

Ceres' surface observed at low phase angles by VIR-Dawn

M. Ciarniello (1), M. C. De Sanctis (1), E. Ammannito (2), A. Raponi (1), F. G. Carrozzo (1), A. Longobardo (1,3), F. Tosi (1), E. Rognini (1), F. Zambon (1), S. Schroeder (4), C. A. Raymond (5), C. T. Russell (6) and the VIR team.
(1) IAPS-INAF, Rome, Italy, (2) ASI, Rome, Italy, (3) DIST, Università Partenope, Naples, Italy, (4) DLR, Berlin, Germany, (5) Jet Propulsion Laboratory, California Institute of Technology, Pasadena, CA, USA, (6) University of California Los Angeles, Earth Planetary and Space Sciences, Los Angeles, CA, USA; (mauro.ciarniello@iaps.inaf.it)

Abstract

We take advantage of low phase angle observations performed by the VIR-Dawn spectrometer to extend the investigation of Ceres' surface phase curve in the opposition effect regime. The Hapke's spectrophotometric model and Monte Carlo simulations are compared to VIR data to infer physical properties of the regolith covering Ceres' surface.

1. Introduction

The opposition effect (OE) is a surge of reflectance commonly detected on the surface of atmosphereless bodies [1,2,3], when observed at low phase angles.
The acquisitions obtained by the Visible and InfraRed mapping spectrometer (VIR [4], 0.25-5.1 μm spectral interval) on-board the Dawn mission, during the Extended Mapping Orbit 4 (XMO4) mission phase, allowed the observation of Ceres' surface down to ~0° phase angle, permitting the characterization of the OE. This set of measurements complements previous observations performed during Dawn mission at Ceres, that covered the 7°-132° phase angle range, and allows to extend the analysis of the Ceres's spectrophotometric properties reported in [5].
Here we report about preliminary results from the analysis of these new set of observations, by means of Hapke's photometric model [1] and Monte Carlo ray-tracing [6].

2. Hapke's model and Ceres's phase curve

In [2] Ceres' spectrophotometric properties have been investigated by means of a simplified Hapke's model following the formulation reported in the equation below:

$$\frac{I}{F} = \frac{w}{4}\frac{\mu_{0eff}}{\mu_{0eff}+\mu_{eff}}\left[\left(1+B(\alpha)\right)p(\alpha) + H\left(w,\mu_{0eff}\right)H\left(w,\mu_{eff}\right) - 1\right]S(i,e,\alpha,\bar{\theta}) \quad (1)$$

with
I/F: radiance factor; *w:* single scattering albedo; *α,i,e:* phase, incidence and emission angles, respectively; *p(α):* single particle phase function (SPPF) modeled with a two-parameter Henyey-Greenstein formulation [1]; *B(α):* Shadow hiding OE function depending on OE amplitude (B_0) and angular width (h); $S(i,e,\alpha,\bar{\theta})$: large scale roughness shadowing function, depending on the average surface roughness slope $\bar{\theta}$; *H(w,x):* Chandrasekhar function; μ_{0eff}, μ_{eff}: cosine of the effective incidence and emission angle, respectively.
Assuming Eq. 1, this can be rearranged as follows:

$$\frac{I/F}{D} = \frac{w}{8}\left[\left(1+B(\alpha)\right)p(\alpha) + H\left(w,\mu_{0eff}\right)H\left(w,\mu_{eff}\right) - 1\right] \quad (2)$$

with $D = \frac{2\mu_{0eff}}{\mu_{0eff}+\mu_{eff}}S(i,e,\alpha,\bar{\theta})$.

We refer to the quantity $\frac{I/F}{D}$ reported in Eq. 2 as Ceres' "phase function" since it is mostly dependent on phase angle, while, given the low albedo of Ceres' surface, dependence on incidence and emission angle through the *H* functions is small.

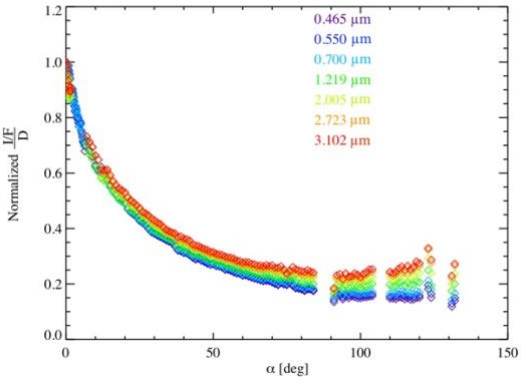

Figure 1. Ceres' phase function at different wavelengths.

In Fig. 1, Ceres' phase function as derived from VIR observations at different wavelengths is shown after normalization at 0°. The curve has been computed by averaging in 0.2° phase angle bins observations from the XMO4 phase for α<7°, while for α>7° the Ceres Approach (CSA), Rotational Characterization 3 (RC3), Ceres Transfer to Survey (CTS), and Ceres Survey (CSS) sequences have been considered (averaged in 1° bins). It can be noted that Ceres' phase function is progressively more forward-scattering for increasing wavelengths.

3. Opposition Effect on Ceres

OE in particulate media is typically attributed to two different mechanisms [1 and references therein]: Shadow Hiding Opposition Effect (SHOE) and Coherent Backscattering Opposition Effect (CBOE). SHOE is produced by a progressive reduction of the visibility of the shadows cast by particles in the top layers of the surface on the ones below, for decreasing phase angles, while CBOE is the effect of the constructive interference at low phase angles between waves propagating in the medium along the same path but in opposite directions. The angular width of SHOE is typically of the order of ~10°-20°, and is considered not to depend on wavelength [1], being mainly driven by light scattered once in the medium. Conversely, CBOE angular width, is typically smaller than SHOE (~1°-2°, [1,2]), and may show wavelength dependence.

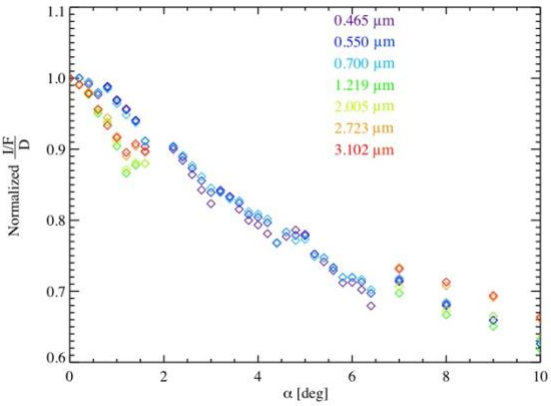

Figure 2. Ceres' phase function, in the 0°-10° phase angle range, at different wavelengths.

In Fig. 2, Ceres' phase curve at small phase angles (α<10°) is shown at different wavelengths. It can be noted that there is no clear spectral dependence of the OE angular width. The observed variability for α<2°, which could be indicative of a contribution from CBOE, in particular at IR wavelengths, is most likely related to the fact that different phase angles sample different regions of the surface, because of the poor observations redundancy. Moreover, the reflectance surge for decreasing α does not show strong evidence of an additional contribution at the smallest phase angles, which could be indicative of CBOE superimposed on the wider SHOE. Although an unambiguous assessment of CBOE requires polarimetry measurements [3], the arguments provided above suggest that SH is the principal mechanism causing OE on Ceres.

4. Hapke's model parameters

XMO4 observations permits to extend the phase angle range investigated in [5] by characterizing the OE region of Ceres' surface phase function, and allow us to derive improved sets of Hapke's model parameters, across the whole VIR spectral range. This is done by fitting the phase function to Eq. 2, and various solutions have been studied, depending on different a priori assumptions on Hapke's model parameters. For example, assuming that B_0 cannot exceed 1, as required from SHOE physics, and $\bar{\theta}$=29° from [5], we derive a preliminary solution at 0.55 µm with $B_0=1$, $h=0.037$, $b=0.40$ $c=0.23$, $w=0.15$. Such a value of w is representative of a low albedo surface, while b and c are compatible with particles characterized by an intermediate level of internal scatterers, according to [7]. Finally, the SHOE angular width (h) can be related to the porosity (P) of the regolith (Eq. 9.26 in [1]) and the derived value corresponds to P=0.91, indicating a highly porous material.

5. Monte Carlo simulations

At the scope to further characterize the porosity of the surface, we perform a preliminary comparison of Ceres' reflectance curve with the output of Monte Carlo (MC) ray-tracing simulations [6]. MC simulations performed for different filling factors of the modeled regolith in the range Φ=0.01-0.3, indicate, as expected, that smaller porosities provide larger SHOE widths, and Ceres' reflectance curve is better matched by MC simulations with Φ between 0.05-0.1, (P=0.9-0.95). This is compatible with the result derived from the Hapke's model.

Acknowledgements

This work is supported by the Italian Space Agency (ASI, ASI-INAF n. I/004/12/1) and NASA. Enabling contributions from the Dawn Instrument, Operations, and Science Teams are gratefully acknowledged.

References

[1] Hapke B.W. (2012), Theory of reflectance and emittance spectroscopy. [2] M. Mishchenko (1992), Astrophys. Space Sci. 194, 327–333. [3] Nelson et al. (2000), Icarus, 147, 545–558. [4] De Sanctis, M. C. et al. (2011), Space Sci. Rev., 163, 329. [5] Ciarniello, M. et al. (2017), A&A 598, A130. [6] Ciarniello et al., (2014). Icarus 237, 293–305. [7] McGuire A. F. and Hapke B. W. (1995), Icarus 113, 134-155.

EPSC Abstracts
Vol. 12, EPSC2018-846, 2018
European Planetary Science Congress 2018

The unusual V-type asteroid (2579) Spartacus

Dagmara Oszkiewicz (1), Agnieszka Kryszczyńska (1), Paweł Kankiewicz (2), Josef Durech (3), Anna Marciniak (1), Nick Moskovitz (4), Brian A. Skiff (4), Stefan Geier (5,6), Grigori Fedorets (7), Ireneusz Włodarczyk (8), Volodymyr Troianskyi (1,9)

(1) Astronomical Observatory Institute, Faculty of Physics, A. Mickiewicz University, Poland (dagmara.oszkiewicz@amu.edu.pl), (2) Institute of Physics, Astrophysics Division, Jan Kochanowski University, Poland, (3) Charles University, Czech Republic, (4) Lowell Observatory, USA, (5) Gran Telescopio Canarias, Spain, (6) Instituto de Astrofísica de Canarias, Spain, (7) Department of Physics, University of Helsinki, Finland, (8) Chorzów Astronomical Observatory, Poland, (9) Astronomical Observatory of Odessa I.I.Mechnikov National University, Ukraine

Abstract

Asteroid (2579) Spartacus is a small V-type object located in the inner main belt (the main delivery region for meteorites). It shows spectral characteristics different from typical values for Vestoids (shifted band centers and deeper absorption bands [1], [2]), which may indicate origin deeper within Vesta then other V-types or a different parent body. We determine physical and dynamical properties of (2579) Spartacus and discuss its possible origin scenarios.

1. Introduction

Most howardite-eucrite-diogenite (HED) meteorites are thought to have originated from the crust of asteroid (4) Vesta. However few show distinct oxygen isotope ratios indicating a different parent body. Among those the Bunburra Rockhole meteorite is particularly interesting. It also shows a distinct oxygen isotope composition ([3], [4]) and thanks to its observed fall, its origin was traced back to the inner main asteroid belt. Bland et al. 2009 suggested that its parent body may still be present in the inner main belt. Due to its distinct spectral features asteroid (2579) Spartacus is a candidate parent body of anomalous HED meteorites such as Bunburra Rockhole.

2. Spin and shape

The pole direction and convex shape models for (2759) Spartacus were obtained using the lightcurve inversion method by [5] [6]. We used 36 lightcurves (27 from the literature, and 9 collected in this work). We obtained a retrograde model with spin axis orientation $\lambda = 312^\circ \pm 5^\circ$, $\beta = -57^\circ \pm 5^\circ$ and a symmetric also retrograde solution $\lambda = 113^\circ \pm 5^\circ$, $\beta = -60^\circ \pm 5^\circ$. The convex shape models are presented in Figs. 1 and 2 respectively. The sidereal period in both models agrees closely to $P_{\rm sid} = 3.63602$ h.

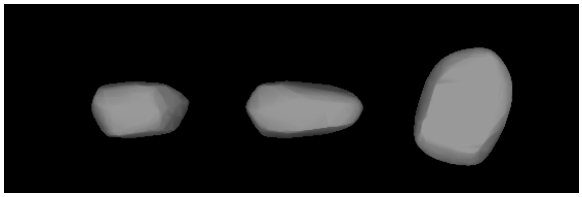

Figure 1: Convex shape model of (2579) Spartacus: Views along the X, Y, Z axis in the asteroid's cartesian frame. Pole coordinates are $\lambda = 312^\circ \pm 5^\circ$, $\beta = -57^\circ \pm 5^\circ$, rotational period $P_{\rm sid} = 3.636028$h

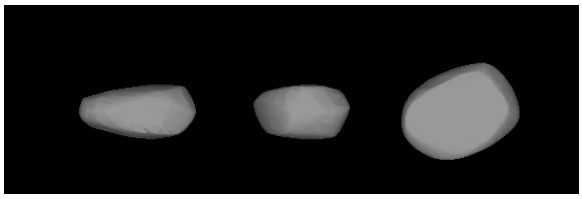

Figure 2: As in Fig. 1, but for a symmetric pole solution $\lambda = 113^\circ \pm 5^\circ$, $\beta = -60^\circ \pm 5^\circ$, $P_{\rm sid} = 3.636027$h.

3. Dynamical properties

To study dynamical evolution of (2579) Spartacus we randomly generated 101 clones with initial orbital elements distributed along the line of variation of orbital elements of (2579) Spartacus. Those clones were then integrated backwards in time for 1 Gy evolving under the influence of the Yarkovsky effect and interacting with the local web of resonances. All the clones had a

radius that of (2579) Spartacus, that is 2.302 km. The remaining initial thermal parameters were selected to resemble that of typical V-types asteroids. The final osculating elements were averaged with Gaussian weights. We have considered four cases: (a) model with prograde pole solution of obliquity $\gamma = 0°$, (b) model with retrograde pole solution of obliquity $\gamma = 180°$, and (c, d) retrograde models with the actual pole solutions. In Fig. 3 we plot the final osculating elements for the different obliquity models at -1Gy, current location of asteroid Vesta and its collisional family is also marked. We find that the retrograde models have a drift direction consistent with the origin in Vesta, but after 1Gy integration time none of the models reach the core of the Vesta family.

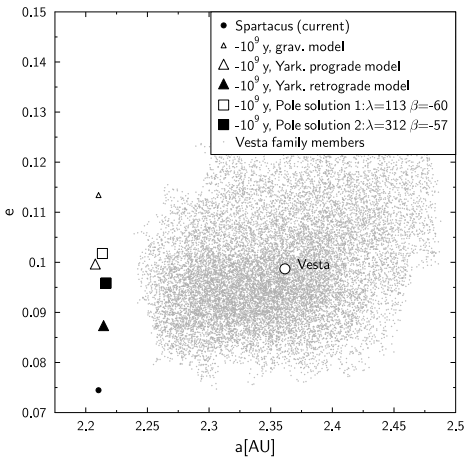

Figure 3: Osculating orbital elements (semi-major axis - a and eccentricity e) at -1Gy for Spartacus assuming different dynamical models and spin orientation.

4. Summary and Conclusions

Based on collected multi-opposition data, we have obtained a retrograde model solution for asteroid (2579) Spartacus. We used estimated size, spin and thermal parameters of Spartacus to investigate its origin and link to (4) Vesta. Dynamical integration shows that the asteroid was drifting from the direction of the Vesta family. We find that at -1Gy the asteroid doesn't yet reach the core of the Vesta family, and longer integration time may be needed for Spartacus to reach the core of the Vesta family. This may indicate that the asteroid originated from an older impact, such as the one that created for example the Veneneia crater (estimated age > 2 Gy).

Acknowledgements

Project supported from National Science Center, Poland grant number 2017/26/D/ST9/00240. Based on observations made with the SMARTS telescope (CTIO), Hall telescope (Lowell Observatory), Nordic Optical Telescope (NOT) and Jacobus Kapteyn Telescope (JKT).

References

[1] Vesta, Vestoids, and the howardite, eucrite, diogenite group: Relationships and the origin of spectral differences Burbine, T. H., Buchanan, P. C, Binzel, R. P, Bus, S. J., Hiroi, T., Hinrichs, JL, Meibom, A and Mccoy, T.J., Meteoritics & Planetary Science, 36, 761–781, 2001.

[2] Ieva S., Dotto E., Lazzaro D.,Perna D., Fulvio D., Fulchignoni M., Spectral characterization of V-type asteroids–II. A statistical analysis Monthly Notices of the Royal Astronomical Society, 455, 2871–2888, 2016.

[3] Spurnỳ p., and Bland P. A., Shrbemý L., Borovička J., and Ceplecha Z., Singelton A., Bevan A. WR, Vaughan D., Towner M. C, McClafferty T. P, and others, The Bunburra Rockhole meteorite fall in SW Australia: fireball trajectory, luminosity, dynamics, orbit, and impact position from photographic and photoelectric records Meteoritics & Planetary Science, 47, 163–185, 2012.

[4] Bland P.A., Spurnỳ P., Towner M.C., Bevan A.W.R., Singleton A.T., Bottke W.F., Greenwood R.C., Chesley S.R., Shrbenỳ L., Borovička J., and others, An anomalous basaltic meteorite from the innermost main belt, Science. 325, 1525–1527, 2009.

[5] Kaasalainen, M. and Torppa, J., Optimization methods for asteroid lightcurve inversion: I. shape determination Icarus, 153, 24–36, 2001.

[6] Kaasalainen M., Torppa, J. and Muinonen, K., Optimization methods for asteroid lightcurve inversion: II. The complete inverse problem Icarus, 153, 37–51, 2001.

EPSC Abstracts
Vol. 12, EPSC2018-863, 2018
European Planetary Science Congress 2018

Experimental Assessment of the High Reflectance Pitted Terrains on Vesta

T. Michalik[1], K. Otto[1], R. Jaumann[1,2], A. Maturilli[1], K. Krohn[1], K.-D. Matz[1], S. E. Schröder[1], K. Stephan[1], [1]German Aerospace Center (DLR e.V.), Rutherfordstr. 2, 12489 Berlin, Germany (tanja.michalik@dlr.de), [2]Freie Universität Berlin, Malteserstr. 74-100, 12249 Berlin, Germany.

Abstract

The pitted terrains around the Marcia crater on Vesta exhibit a higher reflectance and stronger pyroxene band absorptions with respect to their immediate surrounding. Here we present the results of laboratory experiments considered to reveal the process behind this spectral variation. We find that a mere grain size separation effect cannot be the cause for this phenomenon and that it must be of compositional character.

1. Introduction

Pitted terrains on Vesta occur in and/or around relatively young craters and due to their geomorphological appearance and similarity with Martian pitted terrains [1,12] they have been linked to volatile loss [4]. The surface regolith in the broad region of Marcia crater and its surrounding is characterized by a high amount of OH-bearing materials [3] and by a generally lower reflectance and diminished absorption features (likely due to chondritic contamination [e.g. 8,11]).

Within this region, pitted terrains distributed around Marcia crater show a higher reflectance and stronger pyroxene absorptions with respect to their immediate surroundings (Fig. 1), which was previously described in [5] and [6]. The spectral properties match those of more or less pure eucrites which are members of the endogenic HED meteorite group. Some of the pitted terrains also exhibit a local depletion in OH (Fig. 1, lower right panel), as revealed by the 2.8 µm band depth distribution map generated by [2]. The upper panel in Figure 1 shows stronger pyroxene absorptions as greenish colors.

Interestingly, volatile loss is generally not linked to an increased reflectance and enhanced absorption features [e.g., 9,10] and has not been observed on Mars or Ceres. However, (1) particle size segregation, (2) removal of darkening agent and (3) compositional differences due to endogenic or impact related processes might be able to create the observed features on Vesta. Here, we present the primary results of our laboratory sublimation experiments and their implications in order to explain the observed spectral variations.

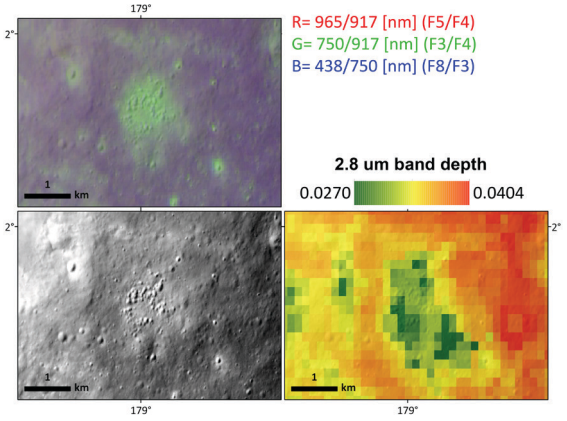

Figure 1: Pitted terrain SW of Marcia. All three panels show the same locality. The lower left panel is a clear filter Framing Camera image at LAMO resolution (~16 m/px). The RGB in the upper panel was generated with FC HAMO data (~60 m/px). Lower right panel was generated by [2] with VIR data.

2. Experimental Setup

All experiments were conducted in the Planetary Spectroscopy Laboratory (PSL) at DLR in Berlin [7]. The reflectance was measured from 0.4 to 1.1 µm in a Bruker 80V spectrometer (biconical, phase angle 30°). We mixed hypersthene as an endogenic analogue (~70-99 wt%) with Murchison chondrite (1 wt%) as well as montmorillonite and carbon black (30 wt%) to create Vestan material analogs.

We placed the samples on top of a water ice layer inside a cylindrical sample container (~5x5 cm), then left it to degas under vacuum (~10^{-5} bar) and a temporarily applied temperature of ~200°C in an emissivity chamber. A metallic lid was placed on top of the sample container (with a small opening of

~3 mm), from where we retrieved the emerged dust (which stuck to the lid) after the experiment.

3. Results

We observed fine-grained particles ("dust") emerging from the container at several sudden events during the experiment. The retrieved dust exhibits a high reflectance but weaker pyroxene absorptions than the original material (labeled "dry mixture" in Fig. 2). The dust contained both endogenic hypersthene particles as well as most of the dark components (i.e., Murchison and carbon black). In the sample container, mostly large hypersthene grains remained (few to none dark components observed). This residual material exhibits low reflectance but strong pyroxene absorptions. We note here that also grains of intermediate size emerged from the sample container but did not get stuck on the lid. We were able to partly retrieve this material from the chamber, which exhibits even larger pyroxene absorptions and higher reflectance than the remaining material in the sample container. However, this emerged material still exhibits a significantly lower reflectance with respect to the original material.

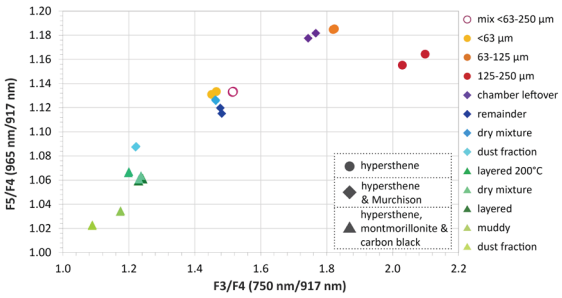

Figure 2: Laboratory data of three different materials (note the different symbols). Note that for all materials, the dust/small grain size fraction has the lowest F3/F4 values (x-axis). However, the pitted terrains on Vesta exhibit higher F3/F4 values than their surroundings. Larger grain size fractions exhibit higher F3/F4 values but much lower reflectance, which is contrary to what we observe on Vesta.

4. Discussion

Our experimental work and the orbital observations imply that grain size segregation and/or the removal of a darkening agent cannot sufficiently explain the spectral behavior of the pitted terrains on Vesta. It is more likely that other, so far undetected compositional differences cause the observed spectral characteristics. As indicated by the depletion of these local areas in OH, the dehydration of phyllosilicates due to heating might play a significant role.

Deposition patterns and geomorphological evidence furthermore suggest that the pitted terrains are associated with the emplacement of Marcia ejecta, which is still ongoing work.

Acknowledgements

This work is part of the research project „The Physics of Volatile-Related Morphologies on Asteroids and Comets". I (T. Michalik) would like to gratefully acknowledge the financial support and endorsement from the DLR Management Board Young Research Group Leader Program and the Executive Board Member for Space Research and Technology as well as Dr. Katharina Otto. Furthermore, I want to acknowledge the possibility to perform the sublimation experiments and reflectance measurements at the PSL at DLR in Berlin.

References

[1] Boyce et al. (2012) Origin of small pits in martian impact craters, Icarus 221, 262-275.

[2] Combe et al. (2015) Reflectance properties and hydrated material distribution on Vesta: Global investigation of variations and their relationship using improved calibration of Dawn VIR mapping spectrometer, Icarus 259, 21-38.

[3] De Sanctis et al. (2012) Detection of widespread hydrated materials on Vesta by the VIR imaging spectrometer on board the Dawn mission, Astrophysical JL, 758:L36.

[4] Denevi et al. (2012) Pitted Terrain on Vesta and Implications for the Presence of Volatiles, Science 338, 246-249.

[5] Giebner et al. (2017a) Pristine crust exposure in Marcia crater on Vesta: new spectral and geomorphological evidence, LPSC XLVIII abstract #1922.

[6] Giebner et al. (2017b) Pitted terrains around Marcia crater on Vesta: strong eucritic absorptions and their implications EPSC abstract #2017-637.

[7] Maturilli & Helbert (2016) The Planetary Spectroscopy Laboratory (PSL): Spectral measurements of planetary analogues from UV to FIR, LPSC XLVII abstract #1986.

[8] McCord et al. (2012) Dark material on Vesta from the infall of carbonaceous volatile-rich material, Nature Letter 491, 83-86.

[9] Poch et al. (2016) Sublimation of water ice mixed with silicates and tholins: Evolution of surface texture and reflectance spectra, with implications for comets, Icarus 267, 154-173.

[10] Pommerol et al. (2015) The SCITEAS experiment: Optical characterizations of sublimating icy planetary analogues, PSS 109-110, 106-122.

[11] Reddy et al. (2012) Delivery of dark material to Vesta via carbonaceous chondritic impacts, Icarus 221, 544-559.

[12] Tornabene et al. (2012) Widespread crater-related pitted materials on Mars: Further evidence for the role of target volatiles during the impact process, Icarus 220, 348-368.

EPSC Abstracts
Vol. 12, EPSC2018-888, 2018
European Planetary Science Congress 2018

High thermal inertia areas on Ceres

[1]**E. Rognini**, [1]M. T. Capria, [1]F. Tosi, [1]M. C. De Sanctis, [1]A. Frigeri, [1]E. Palomba, [1]A. Longobardo, [1]S. Fonte, [2]M. Giardino, [1]F. G. Carrozzo, [1]A. Raponi, [1]M. Ciarniello, [2]E. Ammannito, [3]C. A. Raymond, [4]C. T. Russell

[1]INAF-IAPS Istituto di Astrofisica e Planetologia Spaziali, Via del Fosso del Cavaliere 100, 00133 Roma, [2]ASI Agenzia Spaziale Italiana, Via del Politecnico snc , 00133 Roma, [3]Institute of Geophysics and Planetary Physics, University of California at Los Angeles, 3845 Slichter Hall, 603 Charles E. Young Drive, East, Los Angeles, CA 90095-1567, USA, [4]NASA/Jet Propulsion Laboratory and California Institute of Technology, 4800 Oak Grove Drive, Pasadena, CA 91109, USA

Abstract

We compare theoretical and measured surface temperatures on Ceres. We model surface temperatures with a termophysical code that provides the temperature value as a function of thermal conductivity and roughness (i.e., a measure of topography on the sub-pixel scale). The results suggest high values of thermal inertia in the Haulani crater, and possibly in crater Occator's faculae.

1. Introduction

Thermal inertia is a fundamental parameter that controls surface temperature variations of airless body. Its value is sensitive to the presence of dust, regolith or rock, so this is an indicator of the history and type of the surface material. Ceres and Vesta, the two largest bodies of the main asteroid belt, are important to understand the early stages of solar system and the formation of terrestrial planets. The Visible and InfraRed mapping spectrometer (VIR) [1] onboard the NASA Dawn mission enabled the measurement of surface temperatures of these bodies on their dayside (the instrument is sensitive to daytime temperatures higher than 180 K [2]), and a thermal analysis was performed Vesta's surface, obtaining a broadly regional map of thermal inertia [3]. We have recently carried out a similar analysis for Ceres [4] to determine its average value of thermal inertia. Here, we show the results of the analysis performed on two local-scale areas: the bright faculae found in the floor of crater Occator, and crater Haulani.

2. The method

We derive thermal inertia by comparing VIR-retrieved surface temperatures with theoretical temperatures calculated with a thermophysical model. Local illumination and observing geometry have been derived from a detailed shape model of Ceres. The surface temperature strongly depends on the thermal conductivity of the uppermost surface layer as thick as few cms; the code can simulate different types of material from moondust to bedrock, in ascending order of thermal conductivity. Crater Occator's bright faculae and crater Haulani have been analyzed in this way and for each of them we calculated theoretical daytime temperature profiles, varying the parameters of thermal conductivity and roughness until the measured temperature values were reproduced to within the associated uncertainties.

3. Summary and Conclusions

We find that the thermal inertia in crater Haulani's central mountainous ridge and floor is substantially higher than the average value of Ceres. It should be noted that Haulani is one of the youngest impact craters on Ceres (< 6 Myr, [5,6]) both from a geologic and mineralogical perspective [7]. Its central mountainous ridge and parts of its floor may be substantially compact compared to surrounding terrains, even though it remains unclear why the same behavior is not observed in other comparably young surface features. Although to a lesser extent compared to crater Haulani, the bright faculae found in the floor of crater Occator may also be showing higher-than-average thermal inertia, probably due to locally coarse grain size or roughness; this point is still unclear.

Acknowledgements

VIR is funded by the Italian Space Agency and was developed under the leadership of INAF-Istituto di Astrofisica e Planetologia Spaziali, Rome, Italy. The

instrument was built by Leonardo (Selex-Galileo), Florence, Italy. The authors acknowledge the support of the Dawn Science, Instrument, and Operations Teams. This work was supported by the Italian Space Agency and NASA. We thanks the Dawn Operation Team and the Dawn Science Team.

References

[1] M. C. De Sanctis et al., Space Sci. Rev., **163**, 329–360 (2011), [2] F. Tosi, M. T. Capria, M. C. De Sanctis et al., Icarus, **240**, 36-57 (2014), [3] M. T. Capria, F. Tosi, M. C. De Sanctis, F. Capaccioni et al., Geophysical Research Letters, **41**, 1438-1443 (2014), [4] Rognini, E., Capria, M. T., Tosi, F., et al., EPSC2017, **11** (2017) [5] O'Brien D. P., Walsh K. J., et al., Icarus **239**, 74–84 (2014), [6] Hiesinger H., Marchi S., et al., Science **353** (2016), [7] Tosi et al. Meteoritics & Planetary Science 1–23 (2018)

EPSC Abstracts
Vol. 12, EPSC2018-965, 2018
European Planetary Science Congress 2018

Exploring Ceres geology using Dawn Framing Camera

Guneshwar Thangjam (1), Andreas Nathues (1), Martin Hoffmann (1), Nico Schmedemann (1), Kurt Mengel (2)
(1) MPI for Solar System Research, Göttingen, Germany, (2) Clausthal University of Technology, Clausthal-Zellerfeld, Germany, (thangjam@mps.mpg.de)

Abstract

Despite the advanced geologic exploration of Ceres from Dawn observations, some questions remain open. Here we present several of those, and our approach mainly focusing on Framing Camera color data.

1. Introduction

The Dawn spacecraft, equipped with three scientific instruments (Framing Camera/FC, Visible and Infrared Spectrometer/VIR, Gamma Ray and Neutron Detector/GRaND), has been exploring the geology of dwarf planet Ceres since 2015. The eyes of the Dawn mission, the FC, is used for several scientific purpose, for example, geologic mapping, crater counting, surface topography and surface composition. Constraints on the composition of the surface material are derived from color imagery.

Currently Dawn performs its last mission phase, the extension XM2. This orbit brings the spacecraft closest to the cerean surface ever and thus is expected to deliver further insights and details on the cerean geologic evolution. The new data will likely address the open scientific questions.

2. Insights from FC

The Framing Camera is equipped with a clear filter and seven color filters in the wavelength range from 0.4 to 1.0 µm. It is worth mentioning that though the color data is used to constrain the surface composition, it often does not allow unique conclusions because of rather limited wavelength range that are less diagnostic to cerean composition. However, in combination with VIR spectral data the FCs are a powerful tool to detail compositional units.

Figure 1A shows bright and dark material distribution on Ceres highlighting some of the prominent features [1]. The bright material plays an important role revealing surface and subsurface composition. For example, bright material at Occator crater is the most enigmatic geologic feature on Ceres indicating recent geologic activity, possibly lasting until today [1-4]. Meanwhile, an in depth understanding of the cerean dark material is missing, though the very dark material is of similar importance with the bright material. The spectral properties of bright and dark material are found to be altered, changing over time to the cerean average/background material [1]. Further detailed studies of the bright and dark material would shed light on the aqueous and thermal alteration, maturation, and space weathering processes.

Figure 1B shows the color variation across the cerean surface, along with the spectral variations [Fig. C, D]. The different colors indicate compositional variations and/or unique physical properties, which require careful studies in combination with VIR data. For example, peculiar red slope spectra (increasing reflectance with wavelength) have been noted first by [4], and later on VIR observations identified aliphatic organics at these localities [5]. Again, another type of red spectral sloped material is found at Occator's dome, whose nature is not understood yet [6]. Furthermore, multiple sites with less red spectral slope are reported that might be linked to organics [6].

The spectral variations seen in Fig. 1C-D signify important compositional variations across the surface. The red spectral slope of Occator bright red ('o'), Ernutet red ('e'), Ceres average ('c') and bright ('b') and dark ('d') material are shown, including patches with yellow ('y') and less red ('lr') material in color.

3. Future work

An integrated analysis of FC and VIR data is in progress, and expected to answer some of those open questions.

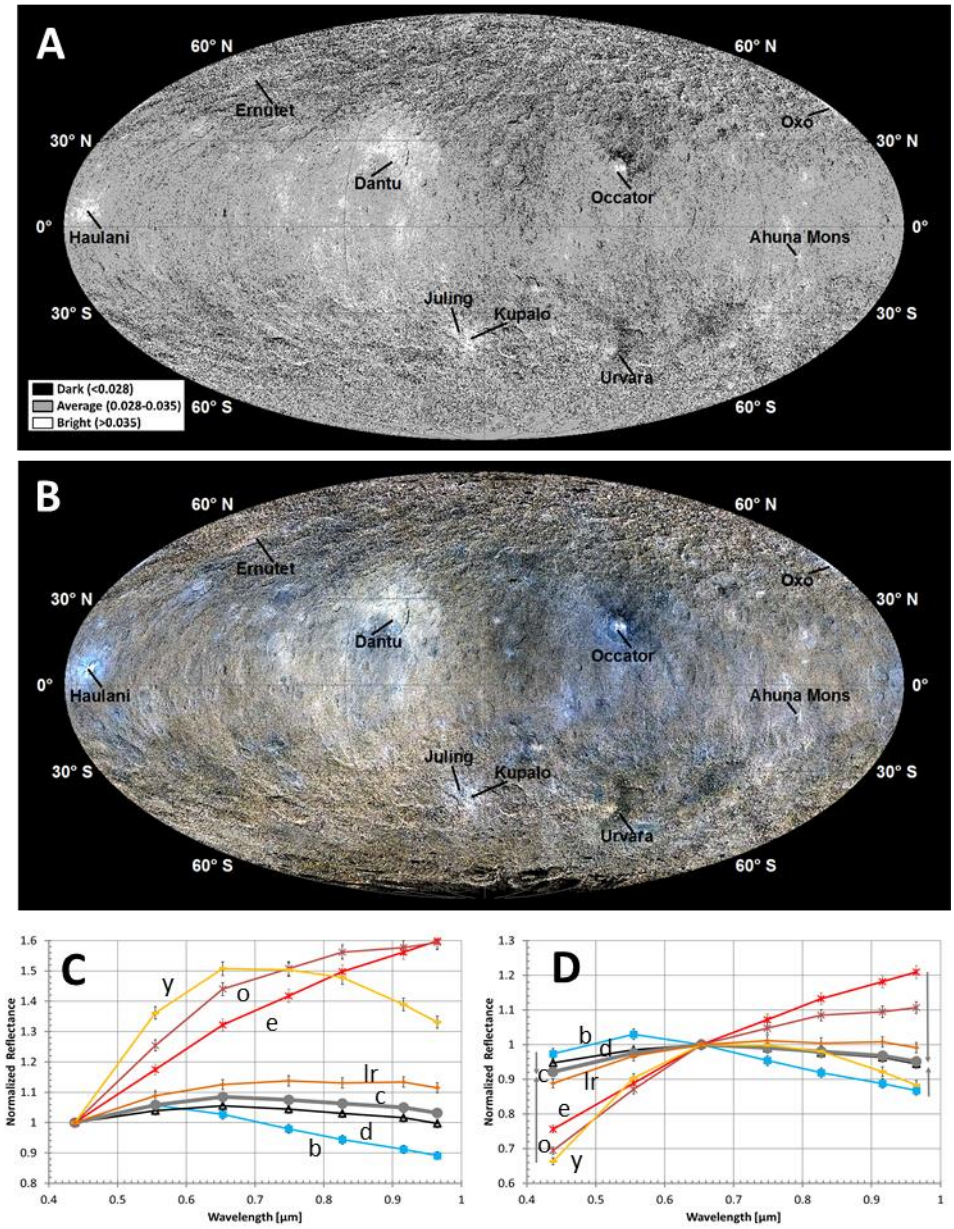

Fig. 1: (A) Bright and dark material distribution on Ceres, (B) Color variation across the surface (R: 0.96, G: 0.65, B: 0.44 μm), (C, D) spectral variability across Ceres surface, normalized at 0.44 μm (C) and 0.65 μm (D). The letters indicate the type of spectra: Occator bright red ('o'), Ernutet red ('e'), Ceres average ('c') and bright ('b') and dark ('d') material, yellow ('y') and less red ('lr') material.

References

[1] Thangjam G. et al. Meteorit. Planet. Sci., in press. [2] Nathues A. et al. Nature, 528,
[3] Thangjam G. et al. ApJL, 833:L25.. [4] Nathues A. et al. 2016, Planet. Space Sci., 134, 122. 237.
[5] De Sanctis M.C. et al. Science, 355, 719. [6] Thangjam G. et al. LPSC 49th, #2025

EPSC Abstracts
Vol. 12, EPSC2018-972-2, 2018
European Planetary Science Congress 2018

The investigation of ridge structures in craters on dwarf planet Ceres

C. Jakob[1], K. A. Otto[1], K. Krohn[1], R. Jaumann[1], F. Preusker[1], T. Roatsch[1], E. Kersten[1], C. T. Russell[2] and C. A. Raymond[3].
(1) German Aerospace Center, Institute of Planetary Research, Berlin, Germany (katharina.otto@dlr.de), (2) University of California LA, Institute of Geophysics, Los Angeles, CA, USA, (3) Jet Propulsion Laboratory, California Institute of Technology, Pasadena, CA, USA.

Introduction: Ceres is the largest and most massive object in the Main Asteroid Belt**,** with a diameter of about 950 km and a mass of 1/3 of the total mass of the asteroid belt. The intact protoplanet is a key to understand the origin and evolution of the terrestrial planets [5]. Especially of interest is the role of water during planet formation. As a differentiated dwarf planet, Ceres is thought to possess a water rich mantle overlying a rocky core [7].

NASA's Dawn spacecraft arrived in orbit around Ceres on March 6, 2015. In multiple orbital phases different types of image data were collected via the on-board Framing Camera (FC), which enabled geologic mapping of the body's surface [1, 6]. Collected image data revealed a surface defined by craters. Some of these craters have ridge structures in their center (example in figure 1). They may be described as elongated central peaks. With the exception of a longish extent, the central ridges morphologically resemble central peaks on Ceres.

The aim of this investigation is to identify and characterize these crater ridges and to observe if their appearance and their shape, orientation and slope are related to any other crater attributes, such as size or depth. By doing so we aim to better understand the process of the formation of ridges in craters on Ceres.

Data: For examination of the crater ridges the high-resolution data from the Low altitude Mapping Orbit (LAMO, 375 km altitude, 5.4 h, FC resolution of 35 m/pixel) and a digital terrain model (DTM) derived from stereo photogrammetry with data from the High Altitude Mapping Orbit (HAMO, 1475 km altitude, 19 h, FC resolution of 140 m/pixel) were used [2, 3, 4].

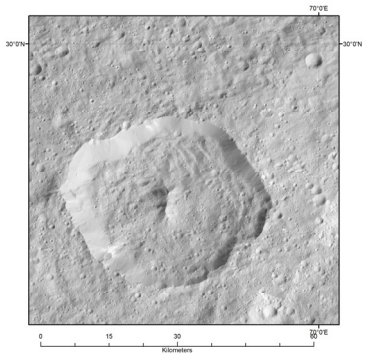

Figure 1: Achita is a ~40 km diameter crater located at 25°N and 65°E.

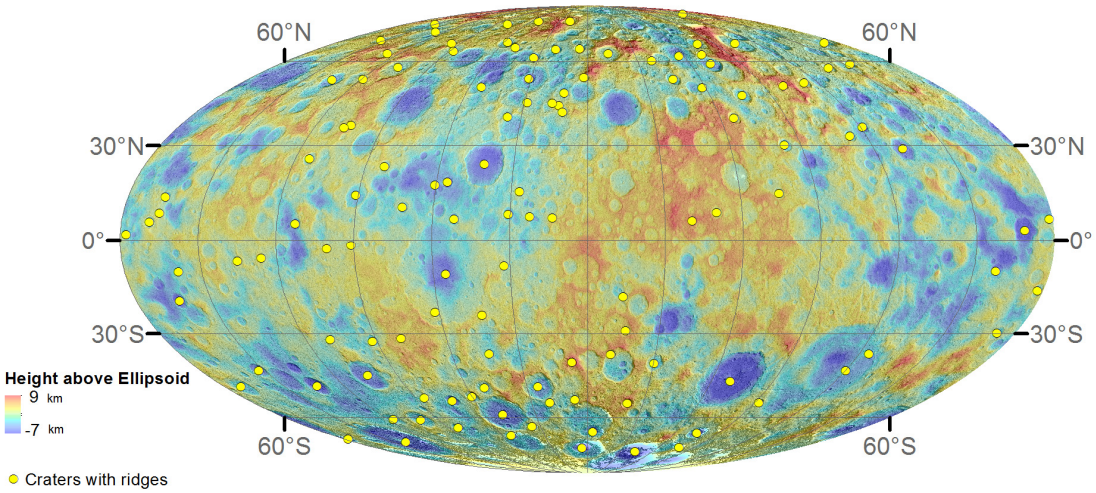

Figure 2: The distribution of craters with ridges on Ceres. The digital terrain model is referenced to a 482 x 445 km ellipsoid.

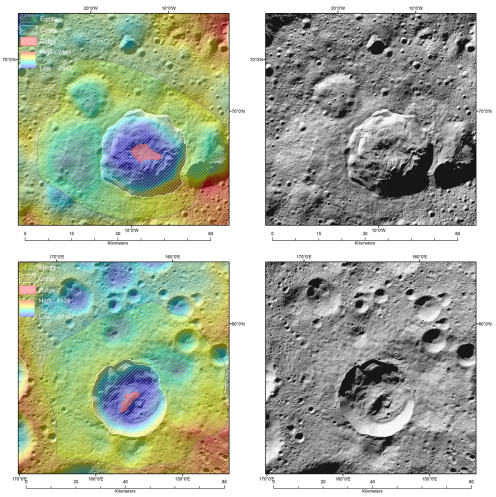

Figure 3: Examples of mapped craters, ridges and ejecta blankets on Ceres.

Results: In total 122 craters with ridges and 29 ejecta blankets have been identified.

The study shows that density distribution of craters with ridges on Ceres is heterogeneously (figure 4). The highest crater density on each hemisphere is found between latitude 60-90°. Highest density in total is found near the polar region on the northern hemisphere.

Length, width and height of ridges tend to become larger with increasing crater diameter. The depth of the craters also correlates with the height of the ridges, length and width of the ridges (figure 5).

The slopes of the ridges correlate with the height of the ridges and also with the width of the ridges. Steeper slopes may indicate younger ridges. Figure 4 shows the distribution of three different intervals of slopes on Ceres.

The analysis of the orientation of a ridge together with the preferential direction of the ejecta deposit of individual craters shows a correlation between both features (figure 6). This investigation suggests that the orientation of a ridge is sensitive to the direction of the impactor hitting Ceres.

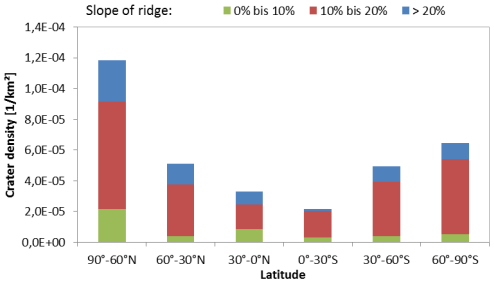

Figure 4: Crater density distribution including distribution of three slope intervals on Ceres.

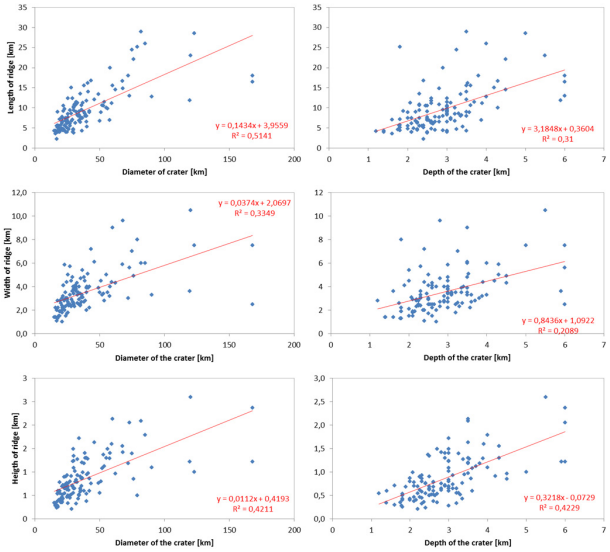

Figure 5: Correlation between size of the ridges and size of the craters.

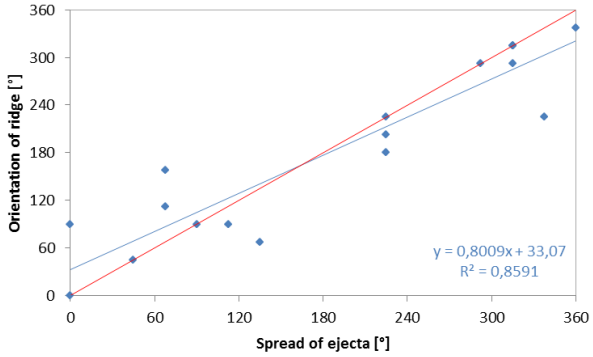

Figure 6: Correlation between the orientation of ridges and the preferential direction of the ejecta deposit. Shown in red is the line of perfect correlation, blue is a linear fit to the data.

References:

[1] Williams, D. A. et al.: Introduction: The geologic mapping of Ceres, Icarus, 2017.

[2] Preusker et al.: Dawn at Ceres: Shape model and rotational state, 47th Lunar and Planetary Science Conference, 2016.

[3] Roatsch, T. et al.: High-resolution Ceres Low Altitude Mapping Orbit Atlas derived from Dawn Framing Camera images, PSS, Vol. 140, pp. 74-792, 2017.

[4] Roatsch, T. et al.: High-resolution Ceres High Altitude Mapping Orbit atlas derived from Dawn Framing Camera images, PSS, Vol. 129, pp. 103-107, 2016.

[5] Russell, C. T. et al.: Dawn: A journey in space and time, PSS, Vol. 52, pp. 465-489, 2004.

[6] Russell, C. T. et al.: Dawn arrives at Ceres: exploration of a small volatile-rich world, Science, 2016.

[7] Thomas, P. C. et al.: Differentiation of the asteroid Ceres as revealed by its shape, Nature, Vol. 437, pp. 224-226, 2005.

EPSC Abstracts
Vol. 12, EPSC2018-998, 2018
European Planetary Science Congress 2018

The issue of secondary craters on Ceres for the example of the Ahuna Mons region

Nico Schmedemann(1), A. Neesemann(2), F. Schulzeck(3), K. Krohn(3), I. von der Gathen(3), K. A. Otto(3), R. Jaumann(2,3), G. Michael(2), G. Thangjam(1), A. Nathues(1), C. A. Raymond(4), C. T. Russell(5)
(1) Max-Planck Institute for Solar System Research, Göttingen, Germany; (2) Institute of Geological Sciences, Freie Universität Berlin, Berlin, Germany; (3) German Aerospace Center, Institute of Planetary Research, Berlin, Germany; (4) JPL, Caltech, Pasadena, CA, USA, (5) University of California, Los Angeles, CA, USA. (schmedemann@mps.mpg.de)

Abstract

Ceres shows an unusual high fraction of crater clusters and crater chains, unprecedented among other asteroidal bodies. It appears that even relatively small craters on the order of 16 km diameter are able to produce a formidable amount of secondary craters stretching out over at least 300 km or 1/10 the Cerean circumference around the crater. Due to Ceres' relatively fast rotation and related Coriolis effects as well as the body's low surface gravity, a significant amount of ejecta is falling back to the surface far from its source crater in a highly asymmetrical distribution. The modelled ejecta distribution pattern predicts certain areas of increased secondary crater density consistent with observations.

1. Introduction

Since March 2015 the Dawn spacecraft is in orbit around dwarf planet Ceres [1]. High resolution imaging data of the Framing Camera (FC) [2] from the low altitude mapping orbit (LAMO) revealed a densely cratered surface [3]. Large basins that likely formed early in the Cerean history are absent or at least muted to a degree of quasi-circular depressions [3], [4]. Crater morphologies very similar to those of the icy satellites in the outer Solar system [3], geophysical investigations [5] as well as spectral observation of volatiles [6] indicate relatively high amounts of water ice that likely governs the rheological behavior of the crustal material [7]. Its properties in conjunction with the Cerean surface gravity in the same range as those of Vesta and the mid-sized Saturnian icy satellites may also support the formation of wide-spread secondary craters. The cratering record of planetary bodies is often used in order to determine their geologic histories. Secondary cratering and other geologic processes can affect the cratering record such that a reasonable age determination becomes challenging. Due to ambiguous reasons Ceres appears to be densely peppered by secondary craters that make surface age determination by the classic approach of analyzing the crater size - frequency distributions of geologic units very difficult. Here we will investigate secondary craters in the region of Ahuna Mons on Ceres.

2. Ejecta Modelling

In order to better understand the spatial distribution of potential secondary craters we model the flight trajectories, impact locations and impact speed of ejecta tracer particles that were ejected from a primary impact crater on Ceres [8]. Previous work demonstrated that the used ejecta model is capable to explain certain features of global scale in color ratio imaging data [8]. The model incorporates crater – projectile scaling [9] and crater ejecta scaling [10]. It takes the rotation of Ceres into account and propagates the particle trajectories as n-body simulation under the influence of the Cerean' gravity as well as the gravitational disturbances of the Sun and the major planets.

3. Results

Figure 1 shows a region north-west of Ahuna Mons with indications of secondary crater chains and crater clusters. In this region, at least two prominent directions (NW – SE; SW – NE) of secondary crater chains can be identified which likely belong to two independent sources. While the source of the chain system in NW-SE direction is unknown, the perpendicular oriented system appears to be consistent with modelled ejecta trajectories of an unnamed crater at 279°E longitude and 23°S latitude.

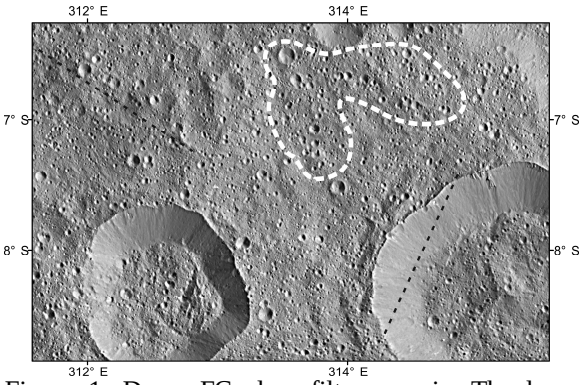

Figure 1: Dawn FC clear filter mosaic. The large crater at the lower left has a diameter of 11 km. The black dashed lines indicate predominant directions of secondary crater chains. The white dashed line outlines an area of unusual high density of similar sized craters, which is characteristic of a secondary crater cluster.

The outlined crater cluster (Figure 1) contains significantly larger craters than the crater chains and requires a larger primary source crater. In fact the presented region is located exactly where the eastward ejected material from Urvara crater is reaching its maximum distance to the east of Urvara. Material that would fly further is overtaken by the rotation of Ceres during its flight time and is impacts closer to its source crater. Figure 2 presents a kernel density map of Urvara tracer particles that indicates regions of higher secondary crater density in warmer colors. In addition, it shows the modelled particle trajectories from an unnamed crater at 279°E / 23°S with about 16 km diameter.

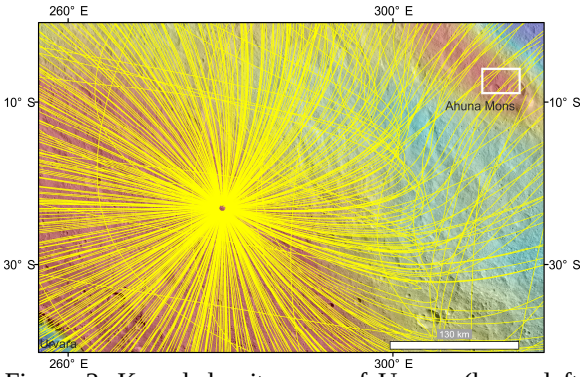

Figure 2: Kernel density map of Urvara (lower left corner) ejecta with warm colors indicating higher probability for secondary cratering and modelled ejecta trajectories (yellow) of a 16 km diameter crater at 279°E /23°S. The position and size of Figure 1 is indicated by a white rectangle close to Ahuna Mons.

4. Conclusions

The modelling of impact crater ejecta can help to identify the source crater of specific populations of secondary crater chains and even secondary crater clusters. In the presented example a set of SW – NE trending secondary crater chains is consistent in its orientation with ejecta trajectories originating from a 16 km diameter crater at 279°E / 23°S. It is surprising that such a small crater at roughly 300 km distance is able to produce so many well visible secondary crater chains. Furthermore, the outlined cluster of relatively large craters near Ahuna Mons is located in a region that is heavily affected by secondary cratering from the 160 km diameter Urvara crater that is located about 560 km to the south – west. Linking the distance of secondary craters with their impact velocity may help to identify a scaling law for secondary projectiles/ craters and to better understand the material properties.

Acknowledgements

This work has been supported by the German Space Agency (DLR) on behalf of the Federal Ministry for Economic Affairs and Energy, Germany, grants 50 OW 1505 (NS, AN) and 50 QM 1301 (GM), and Helmholtz-Gemeinschaft (Helmholtz Association) PD-207 (KK). We thank the Dawn flight team for their excellent job of navigating and maintaining the probe.

References

[1] Russell C. T. et al.: *Science*, 353, 1008 (2016).
[2] Sierks H. et al.: *Space Science Reviews*, 163, 263 (2011).
[3] Hiesinger H. et al.: *Science*, 353, 1003 (2016).
[4] Marchi S. et al.: *Nature Communications*, 7, 12257 (2016).
[5] Ermakov A. et al.: *Journal of Geophysical Research: Planets*, 122, 2267 (2017).
[6] Combe J. P. et al.: *Icarus*, 2017.
[7] Bland M. T. et al.: *Nature Geoscience*, 9, 538 (2016).
[8] Schmedemann et al., *European Planetary Science Congress, 17–22 September 2017*, Vol. 11, EPSC2017-119(2017), Riga, Latvia.
[9] Ivanov B. A.: *Space Science Reviews*, 96, 87 (2001).
[10] Housen K. R. and Holsapple K. A.: *Icarus*, 211, 856 (2011).

EPSC Abstracts
Vol. 12, EPSC2018-1024, 2018
European Planetary Science Congress 2018

Fine-grained Antarctic micrometeorites and weathered carbonaceous chondrites as possible analogues of Ceres surface: implications on its evolution.

Jacopo Nava (1), Cristian Carli (2), Ernesto Palomba (2), Alessandro Maturilli (3) and Matteo Massironi (1)
(1) Università degli studi di Padova – Dipartimento di Geoscienze, Padova, Italy (jacopo.nava@phd.unipd.it) (2) IAPS-INAF, Istituto Nazionale di Astrofisica e Planetologia Spaziali, Roma, Italy (3) Institute of Planetary Research, German Aerospace Center (DLR), Berlin, Germany.

Abstract

IR spectra of several micrometeorites (MMs) and Antarctic weathered carbonaceous chondrites (AWCCs) have been acquired and compared to Ceres spectra. We propose these samples as possible analogues of Ceres. This allowed us to define a more precise composition of Ceres and to suggest a possible evolution of this body.

1. Introduction

Ceres is an icy body with a surface composition close to the carbonaceous chondrites (CCs) [1] that suffered aqueous alteration [2] and geothermal activity [3]. It has been proposed a composition dominated by phyllosilicates, NH_4-phyllosilicates and carbonates plus organic material and opaque minerals [1]. Nevertheless no certain analogue has been found yet in the meteorite collections. For this reason we analysed CCs that suffered strong weathering in Antarctica, possibly the closest terrestrial environment to the surface of Ceres, and fine-grained MMs collected in the Transantarctic Mountains since [4] suggest that they represent C-type asteroid regolith.

2. Results

We selected 5 samples that have NIR spectra close to the average NIR spectra of an area in the Fejokoo quadrangle (Figure 1) labeled as: 5.29; 18c.11; 19b.7; 6.14 and 18c.13. All the MMs analyzed show the 3.3 µm band but only MMs 6.14 and 18c.13 have evident absorptions at 3.9 µm, related to carbonates, and MM 19b.7 has a weak absorption at around 4 µm. MMs 5.29 and 18c.11 show sharp absorption bands at 3.09-3.1 µm, which on Ceres have been attributed to the presence of NH_4-phyllosilicates [1]. Mineralogically MMs 5.29 and 18c.11 are dominated by Ca-Fe pyroxenes often associated with andradite, jarosite and minor olivine. MMs 19b.7, 6.14 and 18c.13 are more weathered and are mainly made of jarosite plus Fe-carbonates and Fe-K sulfides. All of these samples show the constant presence of carbon compound, which can be poorly graphitized C. Phyllosilicates are rare. For what concerns the AWCCs we found the CM2 sample GRA 98005 with weathering grade Ce that had one side exposed to the Antarctic environment, and is thus heavily altered, and one side that has been preserved with a pristine composition. Spectra on the pristine side are flat and almost featureless. On the contrary spectra of the weathered side tend to have a shape close to the average Ceres spectra. This meteorite, on the weathered side, is dominated by Fe-oxides, Ca-Fe carbonates, anidrite and gypsum plus enstatite and forsterite.

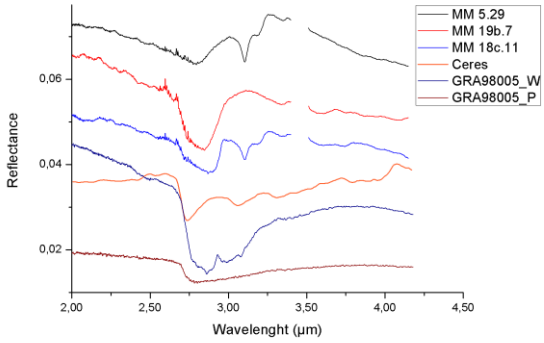

Figure 1: Spectra of MMs and AWCCs compared to Ceres. (GRA98008_W is the weathered side, GRA98005_P is the pristine side).

3. Summary and conclusion

MMs 5.29 and 18c.11 have a composition that is the result of relatively low temperature aqueous alteration <300°C [5], while the other MMs and GRA 98005 show a composition that is mainly the result of rock-ice interaction [6]. On our samples matching the

spectra of Ceres, we didn't find any ammoniated phyllosilicates associated to the 3.1µm band so far. This might suggest that this band can be due to ion-irradiated organics mixed with ice as proposed by [7] or brucite [1]. Nonetheless we cannot rule out the presence of ammonia on Ceres. To better understand the nature of this absorption band further analysis are needed. In addition the analysed samples have low abundances of phyllosilicates compared to what expected on Ceres, probably due to a dehydration caused by heating during entry in atmosphere [4]. In this scenario we can assume that MMs 5.29 and 18c.11 represent products of Fe-alkali-halogen metasomatism that affected and started from the interior of Ceres and expanded very close to the surface as also proposed by [8]. MMs 19b.7, 6.14 and 18c.13 and GRA 98005 are instead representatives of the crust of Ceres that suffered minor hydrothermal activity and suggest that the crust underwent an alteration process similar to the Antarctic weathering. As also stated by [9], the interior of CCs parent bodies (and thus Ceres) were heated up to dehydration temperatures creating H_2 gas that migrated to the surface through cracks and fractures and created vents even with explosive processes [10]. The result is that part of the water sublimated into space and part froze within the crust of Ceres leaving the interior without hydrated minerals. This process may have also depleted the core of some of the main long-term radiogenic sources such as K and enriched the crust with these mobile elements [11]. This heat source on the crust in addition to minor impacts may have melted the water that altered the regolith of Ceres and partially rehydrated materials coming from the underlying layers.

4. Acknowledgements

We aknowledge ANSMET and MNA (Museo Nazionale dell'Antartide) for providing CCs and MMs samples. We thank NASA for development and operations of the Dawn spacecraft. We also thank the instrument teams (Max Plank Institute, DLR, INAF and Planetary Science Institute) for processing of Dawn data. Europlanet 2020 RI has received funding from the European Union's Horizon 2020 research and innovation program under grant agreement No 654208.

References

[1] De Sanctis, M.C., Ammannito, E., Raponi, A., Marchi, S., McCord, T.B., McSween, H.Y., Capaccioni, F., Capria, M.T., Carrozzo, F.G., Ciarniello, M., Longobardo, A., Tosi, F., Fonte, S., Formisano, M., Frigeri, A., Giardino, M., Magni, G., Palomba, E., Turrini, D., Zambon, F., Combe, J.-P., Feldman, W., Jaumann, R., McFadden, L.A., Pieters, C.M., Prettyman, T., Toplis, M., Raymond, C.A. and Russell, C.T.: Ammoniated phyllosilicates with likely outer Solar System origin on (1) Ceres, Nature, Vol. 528, pp. 241-244, 2015..

[2] Neveu, M. and Desch, J.: Geochemistry, thermal evolution, and cryovolcanism on Ceres with a muddy ice mantle, Geophysical Research Letters, Vol. 42, pp. 10,197-10,206, 2015.

[3] Hendrix, A.R., Vilas, F. and Li, J-Y.: Ceres: Sulfur deposits and graphitized carbon, Geophysical Research Letters, Vol. 43, pp. 8920-8927, 2016.

[4] Suttle, M.D., Genge, M.J., Folco, L. and Russel, S.S.: The thermal decomposition of fine-grained micrometeorites, observations from mid-IR spectroscopy, Geochimica et Cosmochimica Acta, Vol. 206, pp. 112-136, 2017.

[5] Krot, A.N., Petaev, M.I., Scott, E.D.R., Choi, B-G., Zolensky, M.E. and Keil, K.: Progressive alteration in CV3 chondrites: More evidence for asteroidal alteration, Meteoritics & Planetary Science 33, pp. 1065-1085, 1998.

[6] Lee, M.R. and Bland, P.A.: Mechanism of weathering of meteorites recovered from hot and cold deserts and the formation of phyllosilicates, Geochimica et Cosmochimica Acta, Vol 68, pp. 893-916, 2004.

[7] Vernazza, P., Mothé-Diniz, T., Barucci, M.A., Birlan, M., Carvano, J.M., Strazzulla, G., Fulchignoni, M. and Migliorini, A.: Analysis of near-IR spectra of 1 Ceres and 4 Vesta, targets of the Dawn mission, Astronomy & Astrophysics, Vol. 436, pp. 1113-1121, 2005.

[8] Castillo-Rogez, J.C. and McCord, T.B.: Ceres's evolution and present state constrained by shape data, Icarus, Vol. 205, pp. 443-459, 2010.

[9] Grimm, R.E. and McSween, H.Y., JR.: Water and the thermal evolution of carbonaceous chondrite parent bodies, Icarus, Vol.82, pp. 244-280, 1989.

[10] Wilson, L., Keil, K., Browning, L.B., Krot, A.N. and Bourcier, W.: Early aqueous alteration, explosive disrutption, and reprocessing of asteroids, Meteoritics & Planetary Science, Vol. 34, pp. 541-557, 1999

[11] Castillo-Rogez, J.C., Matson, D.L., Kargel, J.S., Vance, S.D., McCord, T.B., Johnson, T.V.: Role of hydrothermal geochemistry in the geophysical evolution of icy bodies, Lunar and Planetary Science, 2008.

EPSC Abstracts
Vol. 12, EPSC2018-1201, 2018
European Planetary Science Congress 2018

Floor-Fractured Craters on Ceres

Debra L. Buczkowski (1), Hanna G. Sizemore (2), Michael T. Bland (3), Jennifer E.C. Scully (4), Lynnae C. Quick (5), Kynan H. G. Hughson (6), Paul Schenk (7), Julie Castillo-Rogez (4), Carol A. Raymond (4) and Chris T. Russell (6)

(1) Johns Hopkins Applied Physics Laboratory, Maryland, USA, (2) Planetary Science Institute, Arizona, USA; (3) U.S. Geological Survey Astrogeology, Arizona, USA; (4) NASA Jet Propulsion Laboratory, California, USA; (5) Smithsonian Institute, Washington, DC, USA; (6) University of California, Los Angeles, California, USA; (7) Lunar and Planetary Institute, Texas, USA.

Abstract

Several of the impact craters on Ceres have sets of fractures on their floors. These fractures appear similar to those found within a class of lunar craters referred to as "Floor-Fractured Craters" (FFCs). We have cataloged the Ceres FFCs according to the classification scheme designed for the Moon. An analysis of the d/D ratio for Ceres craters shows that, like lunar FFCs, the Ceres FFCs are anomalously shallow. Large (>50 km) Ceres FFCs are most consistent with Class 1 lunar FFCs, while smaller craters on Ceres are more consistent with Type 4 lunar FFCs. This suggests that Ceres FFCs may similarly be due the intrusion of a low-density material below the craters. While on the Moon (and Mars) the intrusive material is hypothesized to be silicate magma, cryomagmatic intrusions are more likely responsible for the formation of the Ceres FFCs. However, new models suggest that at least some of the FFC fractures may have formed due to the solid state flow of a low-viscosity, low-density material into the crater wall.

1. Introduction

Several of the impact craters on Ceres have patterns of fractures on their floors. These fractures are morphologically similar to those found within a class of lunar craters referred to as Floor-Fractured Craters (FFCs). We present a geomorphic and topographic analysis of the cerean FFCs and propose hypotheses for their formation.

1.1 Data

Geologic analysis was performed using Dawn spacecraft [1] Framing Camera (FC) [2] mosaics from late Approach (1.3 km/px), Survey (415 m/px), the High Altitude Mapping Orbit (HAMO - 140 m/px) and the Low Altitude Mapping Orbit (LAMO – 35 m/px) orbits, including clear filter and color images and digital terrain models derived from stereo images.

2. Lunar floor-fractured craters

Lunar FFCs are characterized by anomalously shallow floors cut by radial, concentric, and/or polygonal fractures [3]. These FCCs have been classified into crater classes 1 through 6, based on their morphometric properties [eg. 3, 4, 5]. The depth vs. diameter (d/D) relationship of the FFCs is distinctly shallower than the same association for other lunar craters [eg. 4, 5]. Models for FFC formation have explained their shallow floors by either floor uplift due to magmatic intrusion below the crater [eg. 3, 4, 5] or floor shallowing due to viscous relaxation [e.g. 6]. However, only magmatic uplift models can explain the degree of floor uplift and the asymmetric nature of the uplift present in several of the FFC morphometric classes [5, 7].

3. Cerean floor-fractured craters

We have cataloged the cerean FFCs according to the classification scheme designed for the Moon. Dantu and Occator craters are the type examples for a Class 1 Ceres FFC, having both radial and concentric fractures at the crater center, and concentric fractures near the crater wall. In the magmatic model presented by [5] these craters represent fully mature magmatic intrusions, with initial doming of the crater center due to laccolith formation resulting in the crater center fractures, while continuing outward uplift of the remaining crater floor results in concentric fracturing adjacent to the crater wall. Other large (>50 km) cerean FFCs which have only linear or radial fractures at the center of the crater (e.g. Azacca, Ezinu and Gaue) are also classified as Class 1 FFCs,

but likely represent a less mature magmatic intrusion, with doming of the crater floor but no tabular uplift.

Smaller craters on Ceres are more consistent with Type 4 lunar FFCs, having less-pronounced floor fractures and v-shaped moats separating the wall scarp from the crater interior. Lunar Class 4 FFCs all have the v-shaped moat, but have three sub-classes defined by the interior morphology [5]. Lociyo crater is an example of a Class 4b FFC, having a distinct ridge on the interior side of its v-shaped moat and subtle fracturing. Meanwhile, Ikapati crater is a potential Class 4a FFC, with both radial and concentric fractures, and a possible moat. Other small cerean craters more closely resemble Class 4c FFCs, with a moat and a hummocky interior, but no obvious fracturing.

An analysis of the d/D ratio shows that, like lunar FFCs, the cerean FFCs are anomalously shallow. We also observe the d/D trend for the Class 1 FFCs is shallower than that for the Class 4 FFCs. This is consistent with the magmatic intrusion models, which suggest that the increased fracturing of Class 1 FFCs is due to increased uplift.

4. Summary and Conclusions

It has been suggested that the cerean FFCs may be a product of the intrusion of a cryomagmatic material below the craters uplifting their floors [9]. A cryovolcanic extrusive edifice has been identified on Ceres [10], and so the hypothesis of cryomagmatic intrusions is credible. Other features, mapped as large domes [9], have been proposed to be possible degraded cryovolcanic edifices [9, 10].

However, there is a second hypothesis for the formation of the large domes. Preliminary models show that an impact into the edge of a layer of low viscosity/low density (LV-LD) material within the heterogeneous crust of Ceres can result in surface deformation due to solid-state flow of the layer [11]. In the models, this surface deformation is expressed as doming into the crater wall [11], but the location of this modeled doming is also consistent with the location of some of the fracturing that we observe in some FFCs, such as Dantu and Occator. This opens the possibility that some of the FFC fractures may have formed due to solid-state flow instead of cryovolcanism.

None of the impact craters that host large domes have fractured floors, although in some locations there are large domes near FFCs (Fig. 4). This anti-correlation suggests that there may be a difference in crustal properties between the locations where the FFCs and the volcanic features form. It is possible that the large domes form where solid state flow has occurred, while the FFCs form where there was cryovolcanism. However, it is also possible that differences in a putative subsurface LV-LD layer could account for changes in the observed surface deformation. Further modeling will need to be performed to determine which process is more consistent with the observed features and what we know of the Ceres surface and interior.

Acknowledgements

Support of the Dawn Instrument, Operations, and Science Teams is gratefully acknowledged. This work is supported by grants from NASA through the Dawn project, and from the German and Italian Space Agencies.

References

[1] Russell, C.T. and Raymond, C.A.: *Space Sci. Rev., 163*, 3-23. 2012.

[2] Sierks H. et al.: *Space Sci. Rev., 163*, 263-328, 2012.

[3] Schultz P.: *Moon, 15*, 241-273, 1976.

[4] Jozwiak L.M. et al.: *JGR 117*, 2012. doi: 10.1029/2012 JE004134.

[5] Jozwiak L.M. et al.: *Icarus 248*, 424-447, 2015.

[6] Hall J.L. et al.: *JGR 86*, 9537-9552, 1981.

[7] Dombard, A. J. and Gillis, J.: *JGR, 106*, 27,901–27,909, 2001. doi: 10.1029/ 2000JE001388.

[8] Schenk et al.: *LPSC XLVII*, abs. 2697, 2016.

[9] Buczkowski D.L. et al.: *Science 353*, 2016. doi: 10.1126/science.aaf4332

[10] Ruesch, O. et al.: *Science 353*, 2016. doi: 10.1126/ science.aaf4286.

[11] Bland M.T. et al.: *LPSC XLIX*, abs. 1627, 2018.

EPSC Abstracts
Vol. 12, EPSC2018-1243-1, 2018
European Planetary Science Congress 2018

The intriguing Tina asteroid family: a compositional investigation

Davide Perna (1,2), Cristina Fanasca (1,3), Simone Ieva (1), Valerio Carruba (4), Elisabetta Dotto (1), Elena Mazzotta Epifani (1), Sonia Fornasier (2), Massimo Dall'Ora (5), Pedro H. Hasselmann (2) and Alvaro Alvarez-Candal (6)

(1) INAF-OAR, Monte Porzio Catone, Italy, (2) LESIA-Observatoire de Paris, France, (3) Università Tor Vergata, Rome, Italy (4) UNESP, Guaratinguetá, Brazil, (5) INAF-OACN, Naples, Italy, (6) ON, Rio de Janeiro, Brazil (davide.perna@inaf.it)

Abstract

The Tina dynamical family is the only family in the asteroid main belt known to be completely embedded in a secular resonance (namely, the ν6) stable island configuration. To investigate the nature of the parent body, identify possible interlopers, space weathering trends or links with meteorites, we obtained visible spectral data (acquired with the FORS2 instrument at the ESO-VLT) of 7 family members, and visible colour indices (acquired with the LRS instrument at the TNG) of further 23 asteroids. Our preliminary results will be presented and discussed.

1. Introduction

The small (~ 100 members), relatively young (~ 140-190 Myr) Tina asteroid dynamical family lies in the middle main belt (a ~ 2.8 au). It is the first case of a ν6 anti-aligned librating family. Such dynamical state limits the maximum eccentricity of Tina members, preventing them from close approaches with Mars and forming a stable island of a new dynamical type. Because of the close relationship with the ν6 secular resonance, the Tina family could be a non-negligible source of Earth meteorites [2], [3].

Asteroid (1222) Tina is considered of "metallic" nature due to its X-type spectrum and moderate (~20%) geometric albedo [1], [4]. Very scarce information is available for the other asteroids belonging to the dynamical family. Such physical characterization is however essential to confirm their common origin from a collisional event and to identify the objects that are possible interlopers. Information about possible links with meteorites and about the space weathering processes which occurred on these asteroids could also be retrieved studying their surface composition.

For this reason, we performed an observational survey of asteroid members of the Tina dynamical family, retrieving visible spectra at the 8.2-m ESO-VLT UT1 (using the FORS2 instrument) and visible colour indices at the 3.6-m TNG (using the LRS instrument).

2. Preliminary data analysis

We obtained the visible spectra of 7 asteroids (Tina, 1998 SV34, 1998 VU19, 2001 FT34, 2001 KV54, 2002 RV27, 2006 GO45) and derived their taxonomic classification. Interestingly, three other asteroids share the X-type classification (and moderate albedo measurements in the literature) with Tina, while two targets present a flat, C-type spectrum (unfortunately, no albedo measurements are available for these bodies). One target presents an intermediate C/X spectrum, and an albedo of ~10%.

The reduction and analysis of the BVRI photometric data obtained for further 23 bodies is currently ongoing.

All of our results will be presented and discussed.

Acknowledgements

DP has received funding from the European Union's Horizon 2020 research and innovation programme under the Marie Sklodowska-Curie grant agreement n. 664931.

References

[1] Bus S. J. & Binzel R. P. Icarus 158, 146 (2002).
[2] Carruba V., MNRAS 408, 580 (2010).
[3] Carruba V. & Morbidelli A., MNRAS 412, 2040 (2011).
[4] Masiero J. R., et al., ApJ 791, 121 (2014).

EPSC Abstracts
Vol. 12, EPSC2018-1254, 2018
European Planetary Science Congress 2018

Revisiting the Cerealia and Vinalia Faculae on Ceres

Adrian Neesemann (1), Stephan van Gasselt (2), Simone Marchi (3), Gregory G. Michael (1), Nico Schmedemann (4), Harald Hiesinger (5), Ralf Jaumann (6), Carol A. Raymond (7), Christopher T. Russell (8)
(1) Freie Universität Berlin, Germany (adrian.neesemann@fu-berlin.de), (2) National Chengchi University, Taipei, Taiwan, (3) Southwest Research Institute, Boulder, CO, (4) Max Planck Institute für Sonnensystemforschung, Göttingen, Germany, (5) Westfälische Wilhelms-Universität, Münster, Germany, (6) German Aerospace Center (DLR), Berlin, Germany, (7) Jet Propulsion Laboratory, Pasadena, CA, (8) University of California, Pasadena, CA

1 Introduction

In February and March 2016, the Dawn Spacecraft [1, 2] has for the first time taken high resolution FC [3] LAMO images at short exposure times of the enigmatic bright deposits located within the fresh Occator crater on Ceres. Since then, not only the bright deposits' (faculae) composition of Na_2CO_3 mixed with $(NH_4)_2CO_3$, NH_4Cl and Mg and Al phyllosilicates [4] but also their formation by cryovolcanic eruptions [5, 6] and salt-water fountains [7] have surprised researchers. In addition, initial analyses yielded incredibly young model formation ages of the Cerealia Facula (CF) and Vinalia Faculae (VF) of only 4 Ma [6] and about 700-760 ka [8], respectively. Here we present the results of our more sophisticated approach to further narrow down the faculae formation ages and explain the uncertainties when age dating such sparsely or even uncratered surfaces.

2 Methodology

Since VF only form deposits of several meters up to few tens of meters thickness [8] and gradually fade with distance (Fig. 2), gathering their areal extent for subsequent age estimates by manual mapping involves a high degree of subjectivity. The areal extent affected by resurfacing by the faculae (and/or crater obliterating extensional tectonics [9]) is, however, crucial as results of our Poisson timing analysis [10] for dating sparsely or even non-cratered surfaces basically depend on the crater-size-dependent impact rate, the area size and the resolution dependent crater recognition limit. Therefore, we calculated the mean reflectance ($(I/F)_{avg.}$ = 0.097) and standard deviation (σ = 0.064) of a mosaic of short exposure FC clear filter data FC59292, FC59290, and FC56966, and defined the faculae as material with a reflectance of $^{+}/_{-}1\sigma$ and beyond $+1\sigma$. The resulting areas and their sizes are depicted in the lower panel of Fig. 2 and are comparable to those of a similar approach by [7]. With the absence of craters larger than 4 px in diameter (~140 m at an avg. LAMO resolution of 35 mpx^{-1}) on VF, we can determine the age probability density functions (PDF) for the respective area sizes and for different chronology models. Moreover, at the time of writing, Dawn, currently in its second extended mission (XM2), is supposed to acquire even higher resolution data of the faculae of about 5 mpx^{-1}. So as a preview, we also calculated the age PDFs given the condition that even no craters larger than 20 mpx^{-1} can be found on the faculae.

3 Results and perspective

We applied statistical image analyses in order to more objectively define the extent of CF and VF for accurately calculating their age PDFs for two versions of the Lunar Derived- (LDM) [11, 12] and five versions of the Asteroid Derived chronology Model (ADM) [13-15], developed for Ceres. Our results confirm and expand earlier age estimates by [8] and demonstrate

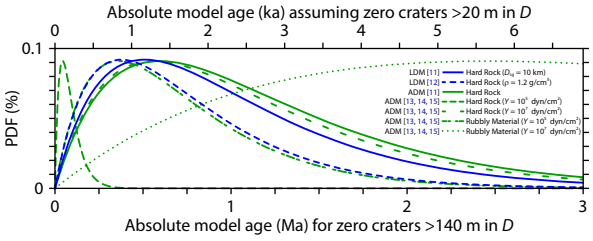

Figure 1: Model age likelihood functions derived for an area the size of all VF (Fig. 2) by evaluating different chronology models developed for Ceres [11-15]. The bottom axis shows the results of our Poisson timing analysis for zero craters larger than 140 m in *D*, while the top axis plots expected results in case even zero craters >20 in *D* are observed in upcoming high resolution XM2 data.

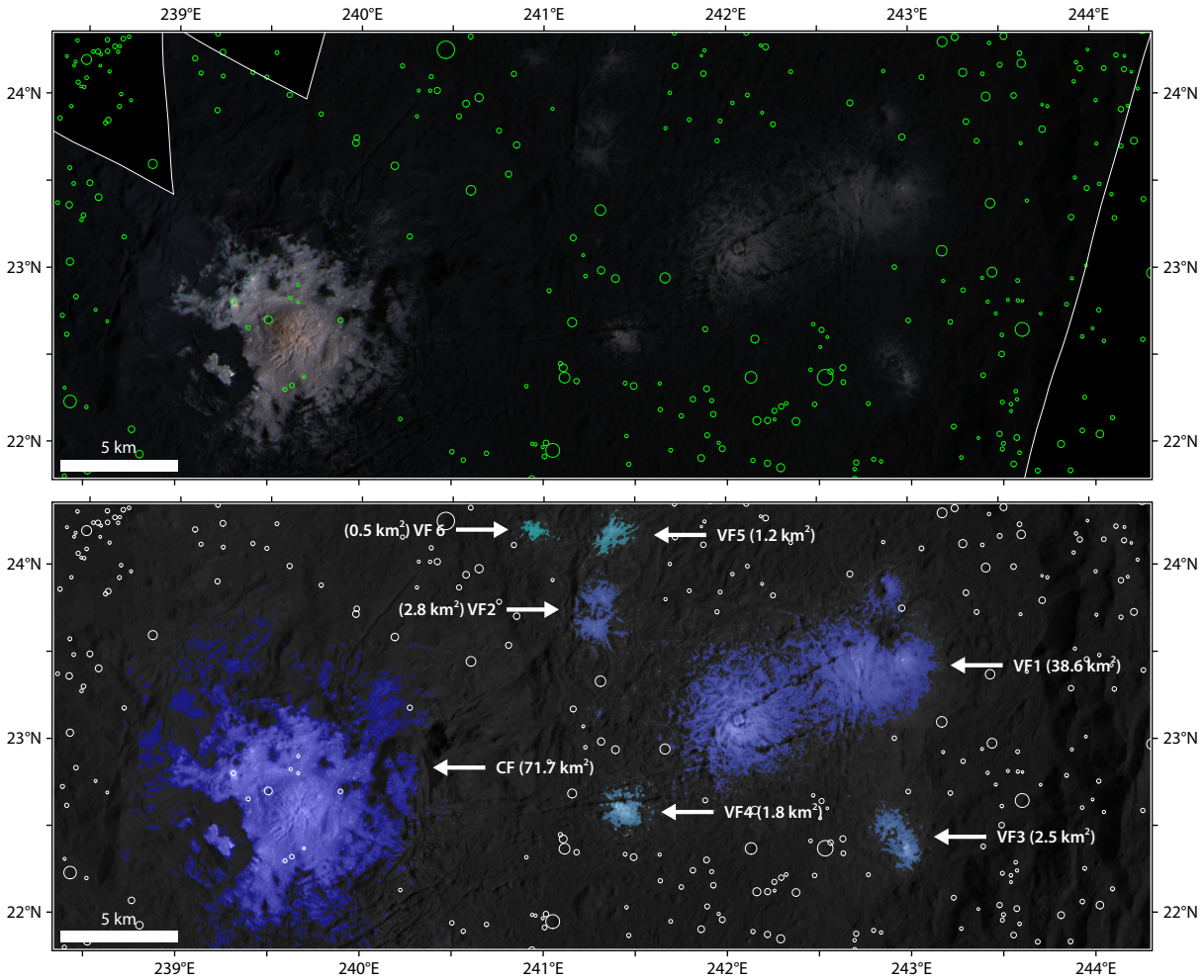

Figure 2: Top: Color composite of the interior of Occator crater using FC LAMO filters F7, F2, and F8 [3] data (R = 0.65 μm, G = 0.55 μm, B = 0.43 μm. Bottom: Mosaic of short exposure FC LAMO clear filter data (FC59292, FC59290, FC57273, FC56966) superimposed by the statistically derived areal extent of the faculae.

how the absence of craters >140 m in *D* around VF theoretically translates into model formation ages of not more than 0.5 Ma. In case Dawn successfully captures the faculae at 5 mpx^{-1} during the XM2, we will be able to confirm our age perspectives for zero craters >20 m in *D* (Fig. 2) of only a few ka or amend the lower crater size boundary for the Poisson timing analysis.

Acknowledgements

We thank the Dawn team for the development, cruise, orbital insertion and operations of the Dawn spacecraft at Ceres. This work was partly supported by the German Space Agency (DLR), Grant 50 OW 1505.

References

[1] Russell et al. (2007), Earth, Moon, and Planets **101**. [2] Russell and Raymond (2011), Space Science Reviews **163**. [3] Sierks et al. (2011), Space Science Review **163**. [4] De Sanctis et al. (2016), Nature **536**. [5] Krohn et al. (2016), Geophysical Research Letters **43**. [6] Nathues et al. (2017), The Astronomical Journal **153**. [7] Ruesch et al. (in press), Icarus. [8] Nathues et al. (in press), Icarus. [9] Buczkowski et al. (in review), Icarus. [10] Michael et al. (2016), Icarus **277**. [11] Hiesinger et al. (2016), Science **353**. [12] Schmedemann et al. (pers. comm.). [13] O'Brien et al. (2014), Planetary and Space Science **103**. [14] Marchi et al. (2014), Planetary and Space Science **103**. [15] Neesemann et al. (in review), Icarus.

EPSC Abstracts
Vol. 12, EPSC2018-1264, 2018
European Planetary Science Congress 2018

Mineralogical and photometric analysis of V-type asteroids

Hissa Medeiros (1), Julia de León (2,3), Daniela Lazzaro (1), Eduardo Rondón (1), Filipe Monteiro (1), Marcel Popescu (2,3), Noemí Pinilla-Alonso (4), Plícida Arcoverde (1), David Morate (2,3), Teresinha Rodrigues (1), Vania Lorenzi (2,5) and Zoe Landsman (6)
(1) Observatório Nacional, Rua Gal. José Cristino 77, 20921-400 Rio de Janeiro, Brazil (hissamedeiros@on.br), (2) Instituto de Astrofísica de Canarias, C/Vía Láctea s/n, E-38205 La Laguna, Spain, (3) Departamento de Astrofísica, Universidad de La Laguna (Spain), (4) Florida Space Institute, UCF, Orlando (USA), (5) Fundación Galileo Galilei – INAF, La Palma (Spain), (6) University of Central Florida, Orlando (USA)

Abstract

Most of the V-types that are known are located in the inner main belt and are members of the Vesta collisional family. The analysis of the photometric and spectroscopic properties of asteroids inside and outside the Vesta family, including V-types in the middle and outer main belt, can answer questions about the existence of differentiated bodies in the asteroid belt and consequently constrain the models of temperature radial extent and variability.

1. Introduction

Basaltic asteroids are taxonomically classified as V-types and their visible-to-near-infrared (VNIR) spectra show two deep absorption bands at 1 and 2 μm, associated with the presence of pyroxene. V-types VNIR spectra are similar to the spectra of HED meteorites and the most representative member of this type of asteroids is (4) Vesta. The majority of V-types are found in the inner asteroid belt as members of the Vesta collisional family, although several have been discovered far from the Vesta family, such as (1459) Magnya [1], showing differences in terms of mineralogy [2, 3]. The existence of such "outsiders" challenged the models of both temperature radial extent and variability during the early Solar System, which generally do not predict melting temperatures in the outer belt.

2. Objectives

The main objective of the present work is to investigate differences among V-types inside and outside Vesta family, using VNIR spectra and photometric phase curves. The spectra are of V-types identified as such using the (Y-J) vs. (J-Ks) color-color plot presented in the Moving Objects VISTA Survey (MOVIS) catalog [4]. The obtained spectra will allow us to confirm their classification as V-types and to infer their detailed mineralogical composition. The phase curves are of V-types classified as such by [5], and being members of diverse populations, in particular: members of the Vesta dynamical family, inner belt with low inclination [6], near-Earth asteroids and middle/outer main belt. The physical parameters obtained from the phase curves will allow to identify similarities and differences among the surface of V-types in different dynamical groups.

3. Methods

The VNIR spectra were obtained using the 2.5m Isaac Newton Telescope (INT) and the 3.6m Telescopio Nazionale Galileo (TNG), both located at El Roque de los Muchachos Observatory (La Palma, Spain), as well as the 3.0m NASA InfraRed Telescope Facility (IRTF), located at Mauna Kea Observatory (Hawaii). The photometric phase curves were obtained at the 1m telescope of the Observatório Astronômico do Sertão de Itaparica (OASI – Itacuruba-PE, Brazil) as part of IMPACTON. The analysis of the spectra allowed to derive several parameters that are diagnostic of mineralogical composition, like the centres and the depths of the absorption bands or the ratio of their areas (BAR), while the phase curves were used to derive the H-G parameters using the program $\text{MAGRED}_{\text{CF}}$.

4. Results

The obtained results seem to indicate that the composition of the asteroids outside the Vesta family is different from that of Vesta itself and from Vesta family members. Interestingly, a V-type asteroid located close to (1459) Magnya shows a significantly large value of the BAR parameter, similar to what is found for Magnya. Phase curves are still under reduction and preliminary results will be shown at the meeting.

Acknowledgements

JdL acknowledges financial support from MINECO under the 2015 Severo Ochoa Program SEV-2015-0548. JdL and DM acknowledge support from the AYA2015-67772- R (MINECO). The work of M. Popescu was supported by a grant of the Romanian National Authority for Scientific Research – UEFISCDI, project number PN-II-RU-TE-2014-4-2199. The present work was carried out with the support of CNPq, Conselho Nacional de Desenvolvimento Científico e Tecnológico – Brazil. The authors thank CAPES, FAPERJ and for diverse fellowships and grants.

References

[1] Lazzaro, D. et al. (2000) Science, 288,2033-2035.

[2] Duffard, D. et al. (2004) Icarus, 171, 120- 132.

[3] Hardersen, P. S. et al. (2014) Icarus, 242, 269-282.

[4] Popescu, M. et al. (2016) A&A, 591, A115.

[5] Ieva, S. et al., 2016, MNRAS, 455, 2871-2888.

EPSC Abstracts
Vol. 12, EPSC2018-1265, 2018
European Planetary Science Congress 2018

Classification of Dawn/VIR data reveals homogeneous surface units on Ceres surface

F. Zambon (1), M.C. De Sanctis (1), G. Carrozzo (1), F. Tosi (1), K. Stephan (2), J.-Ph. Combe (3), K. Krohn (2), M. Ciarniello (1), A. Longobardo (1), E. Palomba (1), A. Raponi (1), G. Thangjam (4), C. T. Russell (5), C.A. Raymond (6), and the Dawn/VIR Team (francesca.zambon@iaps.inaf.it)

(1) INAF-IAPS Istituto di Astrofisica e Planetologia Spaziali, Via del Fosso del Cavaliere 100, 00133 Roma, (2) Institute of Planetary Research, German Aerospace Center (DLR), Berlin, Germany. (3) Bear Fight Institute, Winthrop, WA, USA. (4) Max Planck Institute for Solar System Research, Göttingen, Germany, (5) Institute of Geophysics and Planetary Physics, University of California at Los Angeles, Los Angeles, , USA. (6) NASA/Jet Propulsion Laboratory and California Institute of Technology, Pasadena, USA.

1. Introduction

The NASA Dawn spacecraft [1] orbits around Ceres since March 2015, and is now completing the second extended phase of the mission. The large amount of data acquired by Dawn are fundamental in understanding the chemical and physical properties undergoing on Ceres surface [2]. Dawn's payload is made up of three instruments: the Framing Camera (FC) [3], the Visible and InfraRed mapping spectrometer (VIR) [4], and the Gamma Ray and Neutron Detector (GRaND) [5]. VIR is a key instrument for deciphering Ceres surface mineralogy at unprecedented spatial resolution [4]. The spatial resolution depends on the altitude of the spacecraft over the mean surface, which changes from one phase to another. The main Dawn mission phases at Ceres, in the two-year period 2015-2016, were: Survey (1.1 km/pixel), High Altitude Mapping Orbit (HAMO) (0.38 km/px), and Low Altitude Mapping Orbit (LAMO) (0.095 km/pixel) [1]. After LAMO, the mission was extended to perform a first extended mission phase in 2016-2017, which was divided in a number of sub-phases where the altitude of the spacecraft raised back to ~19,500 km. In 2018, the Dawn spacecraft was finally injected into an elliptical orbit to perform the second and last extended mission phase (XM2). The combination of broad coverage and varying pixel resolution allow both a global analysis and a local study of features of interest. In particular, several VIR-derived mineralogical maps have been produced [6, 7]. The global mineralogy of Ceres is consistent with a large abundance of a low-albedo, carbonaceous chondrite-like spectral endmember, mixed with Mg- and NH_4-bearing phyllosilicates [6, 7] and Mg-carbonates, whereas Ca- and Na-carbonate-rich areas have been identified at the local scale [8]. Outcrops of water ice have also been identified in about ten cases, mainly occurring in shadowed regions inside specific craters [9, 10], as well as at least one organic-rich material unit [11]. Here, we considered VIR data acquired only in the HAMO phase, and we applied clustering and classification methods to define homogeneous compositional units on Ceres surface.

2. Dataset description

The VIR spectrometer acquires data in two distinct channels: the visible channel (0.25 - 1.07 μm), and the infrared channel (1.02-5.1 μm) [4]. The HAMO dataset represents an optimal trade-off between coverage and spatial resolution (~380 m/pixel obtained at broadly regional scale). For this study, we used only VIR data acquired in the infrared channel range, which includes the main absorption bands observed on Ceres. In particular, we selected the 1.0-4.2 μm range, the date were corrected for thermal emission [12] and instrumental artefacts [13], and then corrected for the instantaneous illumination and observation geometry [14]. On the other hand, the 4.5-5.1 μm spectral range was systematically used to perform surface temperature retrieval.

3. Analysis and preliminary results

We applied different clustering and classification methods to VIR-derived spectral indices of Ceres, to emphasize areas displaying similar spectral characteristics based on all of the spectral parameters already used in previous published papers [6, 8] (Fig. 1). First of all, we considered the K-means

unsupervised clustering technique to automatically and non-arbitrarily extract spectral endmembers [15]. Then we used these endmembers to classify the whole dataset, i.e. the entire VIR HAMO coverage of Ceres, by using the Spectral Angle Mapper (SAM) supervised classifier [16]. We selected ten spectral parameters: reflectances at 1.2 and 1.9 μm, spectral slopes computed between 1.16 and 1.81 μm and between 1.81 and 2.25 μm, band depths at 2.7, 3.1 and 4.0 μm, and band centers at 2.7, 3.1 and 4.0 μm, respectively (Fig. 1, upper ten panels).

We first generated global mosaics for each of these spectral indices, which become inputs for our spectral classification. Prior to K-means clustering, we normalized each spectral parameter by its mean value in order to compare different spectral parameters spanning substantially different ranges. We also considered an alternative method to specific selected areas, namely the G-mode unsupervised classification algorithm [17], to compute the statistical weights of the individual variables for specific regions of interest. The classification of VIR-derived spectral parameters for the entire HAMO dataset, indicates that seven homogeneous classes are appropriate enough to represent the global mineralogy of Ceres. In Fig. 1, bottom panel, an example of classification obtained by means of the SAM method is shown. In this presentation, each homogeneous surface unit is marked by a different color, which allows us to display the distribution of the outcome of the classification. A proper selection of spectral parameters, such as band depth and position of the most diagnostic signatures, along with spectral slopes and albedo, demonstrates the existence of substantially different mineralogical units at both regional and local scale. We can then investigate the degree of correlation existing among the spectral parameters, thus identifying those variables that are most important in driving the classification.

Acknowledgments

We thank the Italian Space Agency (ASI, ASI-INAF n. I/004/12/1) and NASA for supporting this work. The VIR instrument was funded and coordinated by the Italian Space Agency and built by Selex ES, with the scientific leadership of the Institute for Space Astrophysics and Planetology, Italian National Institute for Astrophysics, Italy. VIR is operated by the Institute for Space Astrophysics and Planetology, Rome, Italy. Dawn data are archived in NASA's Planetary Data System; VIR spectral data may be obtained at https: //sbn.psi.edu/pds/resource/dwncvir.htm.

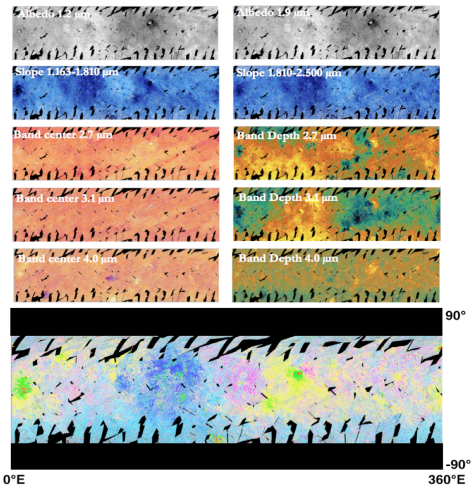

Figure 1: Top: VIR-derived maps of the considered spectral parameters. The meaning of each mosaic is written in white color in the upper left corner. **Bottom:** Result of the K-means unsupervised clustering technique applied to the spectral indices shown in the top panels. Each color corresponds to a homogeneous surface unit resulting from the classification of all of the diagnostic spectral maps considered above.

References

[1] Russell, C.T. and Raymond, C.A., 2011, SSR. [2] Russell, C.T., et al., 2016, Science. [3] Sierks, M. et al., 2011, [4] SSR De Sanctis, M.C., et al., 2011, SSR. [5] Prettyman et al., 2011, SRR [6] Ammannito E. et al., 2016, Science. [7] De Sanctis, M.C. et al., 2015, Nature. [8] Carrozzo, F.G., et al., 2017, Science Adv. [9] Combe, J.-Ph., et al., 2016, Science. [10] Combe, J.-Ph., et al., 2018, Icarus. [11] De Sanctis, M.C., et al., 2017, Science. [12] Raponi, A., et al., 2017, Icarus. [13] Carrozzo, F.G., et al., 2016, RSI. [14] Ciarniello, M., at al., 2017, A&A. [15] Tou and Gonzalez, 1974, Addison-Wesley Pub. Comp. [16] Kruse, F. A., et al., 1993, Remote Sens. Env. [17] Coradini, A., et al., 1977, Comput. Geosci. 3, 85-105.